Nyström-Accelerated Primal LS-SVMs: Breaking the $O(an^3)$ Complexity Bottleneck for Scalable ODEs Learning

Weikuo Wang^{1,2}, Yue Liao^{3,4,*}, Huan Luo^{1,2,*}

¹College of Civil Engineering and Architecture, China Three Gorges University, Yichang, China
²Hubei Geological Disaster Prevention and Control Engineering Technology Research Center, Yichang, China
³College of Basic Medical Sciences, China Three Gorges University, Yichang, China
⁴Hubei Key Laboratory of Tumor Microenvironment and Immunotherapy, Yichang, China
{wkwang, liaoyue, hluo}@ctgu.edu.cn

Abstract

A major problem of kernel-based methods (e.g., least squares support vector machines, LS-SVMs) for solving linear/nonlinear ordinary differential equations (ODEs) is the prohibitive $O(an^3)$ (a = 1 for linear ODEs and 27 for nonlinear ODEs) part of their computational complexity with increasing temporal discretization points n. We propose a novel Nyström-accelerated LS-SVMs framework that breaks this bottleneck by reformulating ODEs as primal-space constraints. Specifically, we derive for the first time an explicit Nyström-based mapping and its derivatives from one-dimensional temporal discretization points to a higher m-dimensional feature space $(1 < m \le n)$, enabling the learning process to solve linear/nonlinear equation systems with m-dependent complexity. Numerical experiments on sixteen benchmark ODEs demonstrate: 1) 10 - 6000 times faster computation than classical LS-SVMs and physics-informed neural networks (PINNs), 2) comparable accuracy to LS-SVMs (< 0.13% relative MAE, RMSE, and $||y - \hat{y}||_{\infty}$ difference) while maximum surpassing PINNs by 72% in RMSE, and 3) scalability to $n=10^4$ time steps with m=50 features. This work establishes a new paradigm for efficient kernel-based ODEs learning without significantly sacrificing the accuracy of the solution.

1 Introduction

Ordinary differential equations (ODEs) are foundational tools for modeling dynamical systems across scientific domains, including physics, engineering, and biology [1, 2]. Classical numerical methods, such as Runge-Kutta schemes and finite difference discretizations, have been the cornerstone of ODE solving due to their rigorous error analysis and convergence guarantees. However, these methods face limitations in achieving satisfactory accuracy with large time steps and incur high computational costs in long-time integration, particularly for stiff ODEs [3]. Recent advances in machine learning (ML) have introduced data-driven paradigms for solving ODEs , such as Physics-Informed Neural Networks (PINNs) [4], neural ODEs [5], and Gaussian process-based solvers [6]. These approaches demonstrate unique advantages in addressing inverse problems, enabling adaptive resolution, and directly incorporating observational data. These capabilities are often challenging for classical techniques.

Among ML-driven methods, kernel-based strategies—particularly Least Squares Support Vector Machines (LS-SVMs) [7]—have emerged as compelling alternatives for solving ODEs. By refor-

^{*}Corresponding authors

mulating the ODEs as a constrained optimization problem in a reproducing kernel Hilbert space (RKHS), LS-SVMs leverage kernel functions to implicitly capture nonlinear dynamics while ensuring regularization against overfitting. This framework has shown success in solving initial/boundary value problems [8] and parameter estimation tasks [9], benefiting from the inherent flexibility and theoretical soundness of kernel methods. However, a critical limitation persists: the computational complexity of kernel-based ODE solvers scales as $O((n+p)^3)$ when solving linear ODEs, and as $O((3n+p-2)^3)$ per Newton iteration in the case of nonlinear ODEs [8], where n is the number of temporal discretization points and p denotes the order of the ODE. This $O(an^3)$ (a=1 for linear ODEs and 27 for nonlinear ODEs) scaling constitutes a major computational bottleneck, rendering traditional LS-SVMs impractical for long-time simulations or fine-grained temporal resolutions, and thereby undermining their utility in large-scale scientific applications.

To address this challenge, we propose a new Nyström-accelerated LS-SVMs framework that reduces the computational complexity to $O((m+p)^3)$ for linear ODEs and $O((m+p+n)^3)$ per Newton iteration for nonlinear ODEs, where $m \ll n$ represents the number of subsampled landmark points. The key innovation of our approach lies in its primal-domain formulation, which strategically integrates the Nyström method—traditionally used for low-rank kernel matrix approximations [10]—into the LS-SVMs optimization procedure. Unlike dual-domain kernel methods, our framework leverages the Nyström approximation to construct an explicit finite-dimensional feature map, enabling efficient computation of high-order derivatives essential for ODE operators. This not only preserves the theoretical benefits of kernel-based regularization but also facilitates a scalable surrogate model for high-resolution ODE systems. The main contributions include: (1) a systematic integration of the Nyström approximation within the LS-SVMs ODE solver, ensuring stability through error-controlled subspace selection; (2) a novel application of the Nyström method to obtain explicit feature mappings and their derivatives, enabling accurate representation of differential operators; and (3) comprehensive numerical validation on sixteen benchmark problems—including stiff and nonlinear systems—demonstrating order-of-magnitude speedups without sacrificing solution fidelity.

This work bridges the gap between the expressive power of kernel methods and the scalability demands of modern scientific computing. By mitigating the $O(an^3)$ complexity barrier, our method unlocks the potential for LS-SVMs to tackle large-scale ODE problems prevalent in multi-physics simulations, biological network modeling, and real-time control systems, where traditional kernel solvers were previously deemed infeasible.

1.1 Related Works

The development of solvers for ordinary differential equations (ODEs) navigates a trade-off between computational efficiency, theoretical robustness, and application flexibility. This section reviews the landscape of numerical, neural, and kernel-based methods, outlining the distinct challenges that motivate our work.

Classical and Enhanced Numerical ODE Solvers: Classical solvers, such as Runge-Kutta schemes [11] and linear multistep methods [12], form the bedrock of ODE simulation. Their principal strength lies in well-established convergence guarantees and explicit error control through adaptive time-stepping. However, their performance is intrinsically linked to the temporal discretization. Stiff ODE systems usually necessitate exceedingly small time steps to maintain stability, leading to prohibitive computational costs in long-time integration. While probabilistic enhancements [13] and Bayesian filters [14] introduce valuable uncertainty quantification, they often exacerbate computational burdens. Even ML-enhanced controllers [15, 16, 17] primarily optimize existing parameters without overcoming the fundamental constraints of discretization, leaving scalability challenges for high-resolution systems largely unresolved.

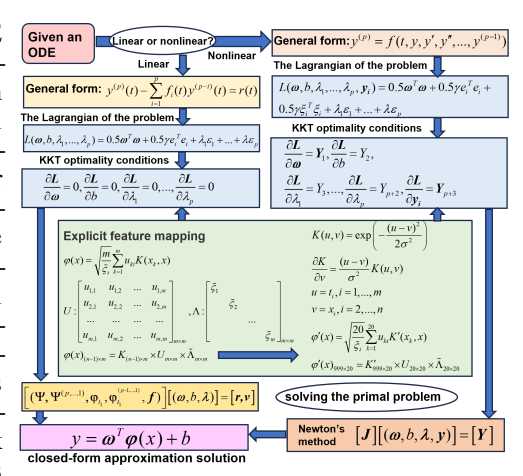
Neural Networks for ODE Systems: Neural network-based approaches represent a paradigm shift towards ODEs solving [18, 19]. Neural ODEs [5] offer a continuous-depth framework that adapts flexibly to irregular time series, and Physics-Informed Neural Networks (PINNs) [4] enable the seamless solution of inverse problems by incorporating physical laws as soft constraints. Despite their flexibility, these methods are prone to convergence issues due to non-convex optimization, often resulting in local minima and unpredictable training outcomes [20]. Furthermore, they can exhibit numerical instability when applied to stiff systems [21] and suffer from spectral bias [22], which impedes the accurate resolution of high-frequency solutions. Although differentiable solvers [23] improve gradient flow, they inherit the iterative cost of the underlying numerical schemes.

Kernel Methods in ODE Solving: Kernel methods, including formulations based on Least-Squares Support Vector Machines (LS-SVMs) [7, 8] and Gaussian processes [6, 24, 25], provide a mathematically rigorous alternative. Operating within Reproducing Kernel Hilbert Spaces (RKHS), they offer convex optimization landscapes that guarantee convergence to a global minimum, avoiding the pitfalls of non-convex training endemic to neural networks. This framework yields closed-form solutions with strong theoretical error bounds, as evidenced in kernel collocation techniques [26]. The primary limitation, however, is their computational scalability: solving the resulting dense linear system requires matrix inversion with $O(an^3)$ complexity, which becomes prohibitive for large-scale or long-time ODE simulations.

Scalability in Kernel-Based ODE Solvers: Accelerating kernel methods has been a central focus in supervised learning, where techniques like the Nyström method [10, 27, 28] and its advanced variants [29, 30] successfully reduce complexity to $O(m^2n)$ for $m \ll n$ landmark points via lowrank matrix approximations. However, these innovations have seen limited translation to the ODE context. Exceptions, such as reduced-rank Kalman filters [31], exploit low-rank structures but remain disconnected from kernelized optimization frameworks like LS-SVMs. Consequently, a significant gap persists: no prior work has systematically reduced the $O(an^3)$ bottleneck of LS-SVMs for ODE solving while preserving their regularization benefits. Our method addresses this by integrating Nyström approximation directly into the LS-SVMs optimization process.

1.2 Novelty and Contributions

Our work bridges the gap between kernelized ODE solvers' theoretical strengths and their practical scalability constraints. In contrast to classical Nyström methods—which are typically applied in the dual formulation of kernel-based classification and regression problems using the kernel trick [10]—our method operates entirely within the primal formulation. This provides an explicit representation of the nonlinear feature mapping and its high-order derivatives, which is specifically tailored to the temporal structure of ODEs and ensures stability in stiff systems (Figure 1). This aligns with trends in datadriven scientific computing but specifically targets the under-explored challenge of $O(an^3)$ complexity in kernel-based ODE solvers. Our framework could be extended to large-scale problems in systems biology, control theory, and multi-agent dynamics, Figure 1: Flowchart of Nyström-accelerated LSwhere traditional kernel-based ODEs solvers were SVMs for Efficient ODE Learning. previously impractical.



Preliminaries

This section describes the problem statement, a short introduction to LS-SVMs (Appendix A.1) for ODEs solving is given to highlight the prohibitive $O(an^3)$ complexity problem considered in this paper. Consider a general p-th order linear/nonlinear ODE with the following form:

$$\mathcal{L}[y] \equiv y^{(p)} = f(t, y, y', \dots, y^{(p-1)}), \quad t \in [t_1, t_n]$$
(1)

where \mathcal{L} represents an p-th order linear/nonlinear differential operator depending on the linear/nonlinear function $f(t, y, y', \dots, y^{(p-1)})$, $[t_1, t_n]$ is the problem domain, t is the input signal, and $y^{(\ell)}(t)$ denotes the ℓ -th derivative of y with respect to $t, \ell \in [0, p]$. The p necessary initial or boundary conditions for solving the above ODE are

IVP:
$$\mathcal{IV}_{\mu}[y] = v_{\mu}$$
, BVP: $\mathcal{BV}_{\mu}[y] = q_{\mu}$, $\mu = 0, \dots, p-1$ (2)

where \mathcal{IV}_{μ} are the initial conditions (all constraints are applied at the initial value of the independent variable i.e., $t=t_1$) and \mathcal{BV}_μ are the boundary conditions (the constraints are applied at multiple values of the independent variable t, typically at the ends of the interval $[t_1, t_n]$ in which the solution is sought). v_{μ} and q_{μ} are given scalars.

When the function $f(t,y,y',\cdots,y^{(p-1)})$ in Eq.(1) is linear, the p-th order ODE to be solved is linear. The optimization problem based on LS-SVMs for learning the p-th order linear ODE can be formulated by the method in Ref [8]. Its solution requires solving a system of (n+p) linear equations with $O((n+p)^3)$ computational complexity. When the function is nonlinear, the p-th order ODE is nonlinear and written in the following form (initial value problems for illustration):

$$y^{(p)} = f(t, y, y', \dots, y^{(p-1)}), \quad y(t_1) = v_0, \dots, y^{(p-1)}(t_1) = v_{p-1}, \quad t_1 \le t \le t_n$$
 (3)

Assume the approximate solution: $\hat{y}(t) = \boldsymbol{\omega}^T \boldsymbol{\varphi}(t) + b$. Additional unknowns y_i are introduced to keep the constraints linear in $\boldsymbol{\omega}$. This yields the following nonlinear optimization problem:

$$\min_{\boldsymbol{\omega}, b, e_i, \xi_i, y_i} \frac{1}{2} \boldsymbol{\omega}^T \boldsymbol{\omega} + \frac{\gamma}{2} \sum_{i=2}^n e_i^2 + \frac{\gamma}{2} \sum_{i=2}^n \xi_i^2$$
s.t. $y^p = \boldsymbol{w}^T \boldsymbol{\varphi}^{(p)}(t_i) = f\left(t_i, y_{t_i}, y'_{t_i}, \cdots, y_{t_i}^{(p-1)}\right) + e_i, \quad i = 2, \dots, n$

$$y(t_1) = \boldsymbol{w}^T \boldsymbol{\varphi}(t_1) + b = v_1, y^{(\ell-1)}(t_1) = \boldsymbol{\omega}^T \boldsymbol{\varphi}^{(\ell-1)}(t_1) = v_\ell, \quad \ell = 2, \dots, p$$

$$y_i = \boldsymbol{w}^T \boldsymbol{\varphi}(t_i) + b + \xi_i, \quad i = 2, \dots, n.$$
(4)

By using classical kernel trick, Eq.(4) can be effectively solved. For detailed mathematical derivation, see Appendix A.2. The nonlinear system, which consists of (3n+p-2) equations with (3n+p-2) unknowns, is solved by Newton's method [32]. For each Newton iteration, solving for unknowns requires the computational complexity of $O((3n+p-2)^3)$. In cases of a long-time interval with more than 10^4 time steps, the prohibitive $O(27n^3)$ part of the computational complexity causes the expensive computations or even may stop the run.

3 Proposed Nyström-accelerated LS-SVMs (NLS-SVMs)

We consider the explicit model, $\hat{y}(t) = \boldsymbol{\omega}^T \boldsymbol{\varphi}(t) + b$, as a closed-form approximation solution to the ODE (i.e., Eq.(1)). A key innovation of the NLS-SVMs approach is its application of the Nyström method to directly approximate the high-dimensional nonlinear feature map $\boldsymbol{\varphi}(t)$ and its higher-order derivatives, enabling the direct substitution of the approximate solution $\hat{y}(t)$ and its derivatives into the governing equation. Therefore, the NLS-SVMs method bypasses the kernel trick, allowing the model parameters to be efficiently estimated in primal form, with computational complexity dependent only on the dimension of the approximated features. Leveraging Mercer's theorem, the derivatives of the feature map $\boldsymbol{\varphi}(t)$ can be analytically expressed using derivatives of the kernel function. To this end, we define the following differential operator:

$$\left[\nabla_c^a K\right](t,s) = \left[\nabla_c^a K(u,v)\right]_{u=t,v=s}, \left[\Omega_c^a\right]_{i,j} = \left.\nabla_c^a \left[K(u,v)\right]\right|_{u=t_i,v=t_j} = \left.\frac{\partial^{c+a} K(u,v)}{\partial u^c \partial v^a}\right|_{u=t_i,v=t_j}$$

where $[\Omega^a_c]_{i,j}$ denotes the (i,j)-th entry of matrix Ω^a_c . Given a long-time interval $\{t_i\}_{i=1}^n$, the Nyström method, as defined in Eq.(34) (Appendix A.3), is employed to construct an explicit finite-dimensional feature mapping $\varphi(t) \in R^m$ with $(m \ll n)$. This allows the model parameters $\omega \in R^m$ and $b \in R$ to be efficiently estimated in the primal space, circumventing the computational burden associated with the dual formulation. Throughout this paper, we adopt the radial basis function (RBF) kernel $K(u,v) = exp(-(u-v)^2/\sigma^2)$. Using the differential relations established in Eq.(5), the first-and second-order derivatives of the kernel function are given by:

$$\nabla_1^0[K(u,v)] = -\frac{2(u-v)}{\sigma^2}K(u,v), \nabla_2^0[K(u,v)] = \left[\frac{4(u-v)^2}{\sigma^4} - \frac{2}{\sigma^2}\right]K(u,v) \tag{6}$$

By extending Eq.(34), the p-th order derivative of the feature map $\varphi(t)$ can be explicitly written as:

$$\varphi_k^{(p)}(t_i) = \sqrt{\hat{\varsigma}_k} \phi_k^{(p)}(t_i) = \frac{\sqrt{m}}{\sqrt{\hat{\varsigma}_k}} \sum_{k=1}^m \hat{\Phi}_{sk} K^{(p)}(t_k, t_i)$$
 (7)

These explicit expressions for the feature map and its derivatives enable the direct numerical treatment of p-th order linear and nonlinear ODEs introduced in Ref [8] and Eq.(4), entirely within the primal framework. As a result, the dominant computational complexity is substantially reduced from $O(an^3)$ to $O(m^3)$ for linear ODEs and $O(n^3)$ for nonlinear ODEs, where $m \ll n$.

3.1 NLS-SVMs for learning p-th Order Linear ODE

Consider the general p-th order linear ODE with initial value problem (IVP) in [8]:

$$y^{(p)}(t) - \sum_{k=1}^{p} f_k(t) y^{(p-k)}(t) = r(t), \quad t \in [t_1, t_n], \quad y(t_1) = v_1, \quad y^{(k-1)}(t_1) = v_k, \quad k = 2, \dots, p$$
(8)

The approximate solution can be obtained by solving the following optimization problem:

$$\underset{\boldsymbol{\omega},b,e_i}{\text{minimize}} \quad \frac{1}{2} \boldsymbol{\omega}^T \boldsymbol{\omega} + \frac{\gamma}{2} \sum_{i=1}^n e_i^2$$
 (9)

s.t.
$$y^{(p)}(t_i) = \boldsymbol{\omega}^T \boldsymbol{\varphi}^{(p)}(t_i) = \boldsymbol{\omega}^T \left[\sum_{k=1}^p f_k(t_i) \, \boldsymbol{\varphi}_i^{(p-k)} \right] + f_p(t_i) \, b + r(t_i) + e_i,, \quad i = 2, \dots, n$$

$$y(t_1) = \boldsymbol{\omega}^T \boldsymbol{\varphi}(t_1) + b = v_1, y^{(\ell-1)}(t_1) = \boldsymbol{\omega}^T \boldsymbol{\varphi}^{(\ell-1)}(t_1) = v_i, \quad \ell = 2, \dots, p$$

Lemma 1: Given a differentiable positive definite kernel function $K : \mathbb{R} \times \mathbb{R} \to \mathbb{R}$, m landmark points subsampled from a dataset of n time points, where $m \ll n$, and a regularization parameter $\gamma \in \mathbb{R}^+$, the solution to optimization problem Eq.(9) is obtained by solving the following primal problem.

$$\begin{bmatrix} \boldsymbol{E} + \mathbf{A} \left(\boldsymbol{\Psi}^{(p)} - \boldsymbol{f_1} \boldsymbol{\Psi}^{(p-1)} - \dots - \boldsymbol{f_p} \boldsymbol{\Psi} \right) & -\mathbf{A} \left(\boldsymbol{f_p} \cdot \mathbf{1} \right) & \boldsymbol{\varphi}^T \left(t_1 \right) & \dots & \left(\boldsymbol{\varphi}^{(p-1)} (t_1) \right)^T \\ \boldsymbol{V} \left(\boldsymbol{\Psi}^{(p)} - \boldsymbol{f_1} \boldsymbol{\Psi}^{(p-1)} - \dots - \boldsymbol{f_p} \boldsymbol{\Psi} \right) & -\boldsymbol{V} \left(\boldsymbol{f_p} \cdot \mathbf{1} \right) & 1 & \dots & 0 \\ \boldsymbol{\varphi} \left(t_1 \right) & 1 & 0 & \dots & 0 \\ & \dots & & \dots & \dots & \dots \\ \boldsymbol{\varphi}^{(p-1)} (t_1) & 0 & 0 & \dots & 0 \end{bmatrix}$$

where
$$\boldsymbol{E} \in \mathbb{R}^{m \times m}$$
 is an identity matrix; $\boldsymbol{\Psi} = [\varphi(t_2), ..., \varphi(t_n)]^T \in \mathbb{R}^{(n-1) \times m}; \boldsymbol{\Psi}' = [\varphi'(t_2), ..., \varphi'(t_n)]^T \in \mathbb{R}^{(n-1) \times m}; \boldsymbol{\Psi}'^{(p)} = [\varphi'(t_2), ..., \varphi'(t_n)]^T \in \mathbb{R}^{(n-1) \times m}; \boldsymbol{\Psi}^{(p)} = [\varphi'(t_2), ..., \varphi'(t_n)]^T \in \mathbb{R}^{(n-1) \times m}; \boldsymbol{f}_1 = [f_1(t_2), ..., f_1(t_n)]^T \in \mathbb{R}^{n-1}; \boldsymbol{f}_p = [f_p(t_2), ..., f_p(t_n)]^T \in \mathbb{R}^{n-1}; \boldsymbol{1} = [1, ..., 1]^T \in \mathbb{R}^{n-1}; \boldsymbol{\varphi}(t_1) \in \mathbb{R}^{1 \times m}; \boldsymbol{\varphi}^{(p)}(t_1) \in \mathbb{R}^{1 \times m}; \boldsymbol{A} = \gamma[(\boldsymbol{\Psi}^{(p)} - \boldsymbol{f}_1 \boldsymbol{\Psi}^{(p-1)} - ... - \boldsymbol{f}_p \boldsymbol{\Psi}]^T \in \mathbb{R}^{m \times (n-1)}; \boldsymbol{V} = \gamma[-\boldsymbol{f}_p \boldsymbol{1}]^T \in \mathbb{R}^{1 \times (n-1)}; \boldsymbol{r} = [r(t_2), ..., r(t_n)]^T \in \mathbb{R}^{n-1}; \boldsymbol{\omega} \in \mathbb{R}^{m \times 1}.$ See Appendix A.4 for proof.

3.2 NLS-SVMs for Learning p-th Order Nonlinear ODE

We establish a new paradigm based on NLS-SVMs for solving Eq.(4).

Lemma 2: Given a differentiable positive definite kernel function $K: \mathbb{R} \times \mathbb{R} \to \mathbb{R}$, m landmark points subsampled from a dataset of n time points, where $m \ll n$, and a regularization parameter $\gamma \in \mathbb{R}^+$, the solution to optimization problem Eq.(4) is given by solving the following primal problem.

$$\begin{bmatrix} \frac{\partial Y_{1}}{\partial \omega} & \frac{\partial Y_{1}}{\partial b} & \frac{\partial Y_{1}}{\partial \lambda_{1}} & \dots & \frac{\partial Y_{1}}{\partial y_{i}} \\ \frac{\partial Y_{2}}{\partial \omega} & \frac{\partial Y_{2}}{\partial b} & \frac{\partial Y_{2}}{\partial \lambda_{1}} & \dots & \frac{\partial Y_{2}}{\partial y_{i}} \\ \frac{\partial Y_{3}}{\partial \omega} & \frac{\partial Y_{3}}{\partial b} & \frac{\partial Y_{3}}{\partial \lambda_{1}} & \dots & \frac{\partial Y_{2}}{\partial y_{i}} \\ \dots & \dots & \dots & \dots & \dots \\ \frac{\partial Y_{p+3}}{\partial \omega} & \frac{\partial Y_{p+3}}{\partial b} & \frac{\partial Y_{p+3}}{\partial \lambda_{1}} & \dots & \frac{\partial Y_{p+3}}{\partial y_{i}} \end{bmatrix} \begin{bmatrix} \omega \\ b \\ \lambda_{1} \\ \dots \\ \lambda_{p} \\ y_{i} \end{bmatrix} = \begin{bmatrix} Y_{1} \\ Y_{2} \\ Y_{3} \\ \dots \\ Y_{p+2} \\ Y_{p+3} \end{bmatrix}$$

$$(11)$$

where $Y_1 \in \mathbb{R}^{m \times 1}$; $Y_2 \in \mathbb{R}^{1 \times 1}$; $Y_3 \in \mathbb{R}^{1 \times 1}$;...; $Y_{p+2} \in \mathbb{R}^{1 \times 1}$; $Y_{p+3} \in \mathbb{R}^{(n-1) \times 1}$. The nonlinear system, which consists of equations with unknowns $(\omega, b, \lambda_1, ..., \lambda_p, y_i) \in \mathbb{R}^{(m+n+p)}$, is solved by Newton's method. While more efficient iterative schemes ([33, 34, 35]) exist, their exploration falls outside the scope of this paper. It is worth noting that when learning a class of p-th order nonlinear ODEs, the changes in the ODEs primarily affect the $\frac{\gamma}{2}(\omega^T \varphi^{(p)}(t_i))$

 $f(t_i,y_{t_i},y'_{t_i},\cdots,y_{t_i}^{(p-1)})\Big)^T\Big(\boldsymbol{\omega}^T\boldsymbol{\varphi}^{(p)}(t_i)-f(t_i,y_{t_i},y'_{t_i},\cdots,y_{t_i}^{(p-1)})\Big) \text{ function, as indicated by the Lagrangian loss function. Therefore, the Jacobian matrix needs to be updated based on the derivation of the four functions <math>\frac{\partial \mathbf{Y}_1}{\partial \boldsymbol{\omega}}$, $\frac{\partial \mathbf{Y}_1}{\partial y_i}$, $\frac{\partial \mathbf{Y}_{p+3}}{\partial \boldsymbol{\omega}}$ and $\frac{\partial \mathbf{Y}_{p+3}}{\partial y_i}$. See Appendix A.5 for proof.

Convergence analysis: Since the tunable parameters (i.e., regularization parameter γ and kernel parameter σ^2) in the nonlinear system Eq.(11) influence the structure of the Jacobian matrix, we theoretically analyze their impact on the convergence behavior of the Newton solver.

Theorem: Consider the system of nonlinear equations in Eq.(11) represented by $F(x; \sigma^2, \gamma) = 0$, where $F: \mathbb{R}^N \to \mathbb{R}^N (N=m+n+p)$ depends on a kernel parameter σ^2 and a regularization parameter γ . Let $J_F(\boldsymbol{x}; \sigma^2, \gamma)$ denote its Jacobian matrix. Assume a solution \boldsymbol{x}^* exists such that $F(\boldsymbol{x}^*; \sigma^2, \gamma) = 0$. The Newton iteration is given by:

$$\boldsymbol{x}_{k+1} = \boldsymbol{x}_k - [J_F(\boldsymbol{x}_k; \sigma^2, \gamma)]^{-1} F(\boldsymbol{x}_k; \sigma^2, \gamma)$$
(12)

Suppose the following conditions hold in a ball $B(x^*, \delta)$ of radius $\delta > 0$ around x^* :

1. Lipschitz continuity of the Jacobian: There exists a constant $L(\sigma^2, \gamma) > 0$ such that

$$||J_F(\boldsymbol{x}; \sigma^2, \gamma) - J_F(\boldsymbol{y}; \sigma^2, \gamma)|| \le L(\sigma^2, \gamma) ||\boldsymbol{x} - \boldsymbol{y}||, \quad \forall \boldsymbol{x}, \boldsymbol{y} \in B(\boldsymbol{x}^*, \delta)$$
(13)

2. Bounded inverse of the Jacobian: The Jacobian matrix $J_F(x; \sigma^2, \gamma)$ is non-singular for all $x \in B(x^*, \delta)$, and there exists a constant $\beta(\sigma^2, \gamma) > 0$ such that

$$\|[J_F(\boldsymbol{x};\sigma^2,\gamma)]^{-1}\| \le \beta(\sigma^2,\gamma), \quad \forall \boldsymbol{x} \in B(\boldsymbol{x}^*,\delta)$$
(14)

Then, for any initial guess $x_0 \in B(x^*, \delta)$ satisfying

$$\|\boldsymbol{x}_0 - \boldsymbol{x}^*\| < \min\left(\delta, \frac{1}{K}\right), \text{ where } K = \frac{1}{2}\beta(\sigma^2, \gamma)L(\sigma^2, \gamma)$$
 (15)

the iteration converges quadratically to $m{x}^*$, with the error $m{e}_k = m{x}_k - m{x}^*$ satisfying:

$$\|e_{k+1}\| \le K \|e_k\|^2 \tag{16}$$

Proof: According to Eq.(12), the error at the next step $e_{k+1} = x_{k+1} - x^*$ can be expressed as (parameters γ and σ^2 are omitted for clarity):

$$\boldsymbol{e}_{k+1} = \boldsymbol{e}_k - [J_F(\boldsymbol{x}_k)]^{-1} F(\boldsymbol{x}_k) = [J_F(\boldsymbol{x}_k)]^{-1} (J_F(\boldsymbol{x}_k) \boldsymbol{e}_k - (F(\boldsymbol{x}_k) - F(\boldsymbol{x}^*)))$$
 The term $F(\boldsymbol{x}_k) - F(\boldsymbol{x}^*)$ is estimated using Taylor expansion with $F(\boldsymbol{x}^*) = 0$:

$$F(\boldsymbol{x}_k) - F(\boldsymbol{x}^*) = \int_0^1 J_F(\boldsymbol{x}^* + t\boldsymbol{e}_k) \boldsymbol{e}_k dt$$
(18)

Substituting this back yields:

$$e_{k+1} = [J_F(x_k)]^{-1} \left(\int_0^1 [J_F(x_k) - J_F(x^* + te_k)] e_k dt \right)$$
(19)

Taking norms and applying the Lipschitz condition (Eq.(13)) to the integrand gives:

$$||J_F(x_k) - J_F(x^* + te_k)|| \le L||e_k - te_k|| = L(1-t)||e_k||$$
 (20)

The integral $\int_0^1 (1-t)dt = 1/2$. Then, applying the bound on the inverse of the Jacobian (Eq.(14)), $||[J_F(\boldsymbol{x}_k)]^{-1}|| \leq \beta$, we obtain the final result:

$$\|e_{k+1}\| \le \beta \cdot \frac{L}{2} \|e_k\|^2 = K \|e_k\|^2$$
 (21)

Implications: The convergence rate is governed by the product $\beta(\sigma^2, \gamma)L(\sigma^2, \gamma)$, which is jointly influenced by the parameters γ and σ^2 . Here, the regularization parameter γ ensures the non-singularity of the Jacobian, while the kernel parameter σ^2 controls the smoothness of F. A larger σ^2 generally reduces the Lipschitz constant L, thereby promoting convergence at the potential cost of oversmoothing. Consequently, a careful balance between σ^2 and γ is critical to achieving an optimal trade-off among convergence speed, solution accuracy, and numerical stability.

Computational complexity reduction: The computational complexity of the proposed NLS-SVMs method, as indicated in Eq.(10) and Eq.(11), is substantially reduced compared to traditional LS-SVMs ODE solvers. It scales with the dimension m ($m \ll n$) of the high-dimensional feature $\varphi(t_i)$. For linear ODEs, it decreases from $O((n+p)^3)$ to $O((m+p)^3)$, while for nonlinear ODEs, the per-Newton-iteration complexity is lowered from $O((3n+p-2)^3)$ to $O((m+p+n)^3)$. Empirical analysis demonstrates that the proposed approach significantly enhances computational efficiency while preserving prediction accuracy. Moreover, the memory requirement for linear ODEs decreases from $O((n+p)^2)$ to $O((m+p)^2)$ and for nonlinear ODEs decreases from $O((3n+p-2)^2)$ to $O((m+n+p)^2)$. Appendix A.6 covers the initial value problem (IVP) for the first-order linear ODE, Appendix A.7 presents the IVP and boundary value problem (BVP) for the second-order linear ODE, and Appendix A.8 provides the derivations for the first-order nonlinear ODE with IVP.

4 Numerical experiments

This section evaluates the performance of the proposed method using sixteen benchmark ODE problems (see Appendix B.1). These include six first-order, nine second-order, and one fourth-order ODE, covering a wide range of common types such as stiff, linear, nonlinear, and singular ODEs, as well as ODEs with time-varying input signals, undamped free vibration, and higher-order dynamics. Prior to the performance evaluation, we conducted a preliminary analysis involving kernel function selection and sampling strategies across all benchmark problems. Convergence behavior was further examined using Problem 4, a representative nonlinear ODE. Additionally, a comprehensive comparative study will be performed against suitable baseline models to thoroughly assess the efficacy of the proposed approach. All numerical experiments in this study were conducted on a computer system equipped with an Intel(R) Core(TM) i9-14900HX processor, 32 GB of RAM. Source code is available at: https://github.com/AI4SciCompLab/NLS-SVMs.

RBF kernel justification: The selection of the kernel function plays a critical role in the proposed methodology, as it directly governs the model's capacity to capture nonlinear patterns. To illustrate this, we examine Problem 1 as a representative case. As shown in Figure 2, the radial basis function (RBF) kernel projects samples into an infinite-dimensional feature space, offering universal approximation capabilities and robustness to variations in data scale. In comparison to linear and polynomial kernels, the RBF kernel demonstrates superior stability and accuracy when applied to complex nonlinear systems (see results for Problems 4, 5, 6, 14 and 15 in Table 4). Consequently, the RBF kernel is adopted in all subsequent experiments. Both the NLS-SVMs and the classical LS-SVMs are tuned via two hyperparameters: the kernel

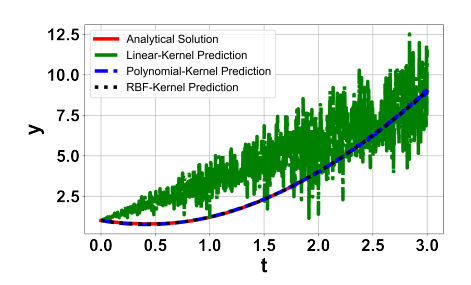


Figure 2: Numerical results for Problem 1 using the Linear, Polynomial and RBF kernel within the NLS-SVMs framework.

bandwidth σ^2 and regularization coefficient γ . A comprehensive quantitative analysis of kernel performance across all benchmark problems is provided in Appendix B.3 (Table 4).

Sampling strategy analysis for Nyström land-marks: To assess the influence of sampling strategy on the performance of the proposed NLS-SVMs method, we evaluate three distinct approaches that are equidistant sampling, ran-

Table 1: Performance comparison of NLS-SVMs with different sampling strategies on Problem 1

| ODEs | Model | MAE | RMSE | $ y - \hat{y} _{\infty}$ | Time/s |
|------|----------------|-----------------------|-----------------------|----------------------------|--------|
| P 1 | Random | 8.70×10 ⁻⁴ | 1.06×10 ⁻³ | 3.06×10 ⁻³ | 0.52 |
| | Leverage score | 7.94×10 ⁻⁴ | 9.47×10 ⁻⁴ | 1.87×10 ⁻³ | 0.64 |
| | Equidistant | 7.94×10 ⁻⁴ | 9.47×10 ⁻⁴ | 1.87×10 ⁻³ | 0.55 |

dom sampling, and leverage score sampling. The analysis for Problem 1, summarized in Table 1, reveals that all three sampling methods achieve a comparable level of prediction accuracy. However, equidistant sampling demonstrates notable advantages in computational efficiency and error reduction. Specifically, it improves computational speed by approximately 16% compared to leverage score sampling and reduces the RMSE by about 10.66% relative to simple random sampling. Comprehensive numerical results evaluating these sampling strategies across all benchmark problems are available in Appendix B.3 (see Table 5). These results demonstrate that the equidistant sampling strategy delivers robust and superior performance. It either matches or surpasses the other methods in the majority of test cases, particularly in challenging scenarios such as stiff systems (e.g., Problem 3), second-order ODEs (e.g., Problems 8, 9, 10, and 12), and problems with singularities (e.g., Problem 13). Furthermore, equidistant sampling exhibits exceptional stability, maintaining consistently low error levels across the entire test cases. While the computational efficiency is generally comparable across all methods, the equidistant strategy frequently attains superior accuracy without incurring a substantial computational penalty. In many cases, its runtime is nearly identical to that of the fastest alternative. These collective results indicate that the equidistant sampling strategy provides an optimal balance between numerical precision and computational expense.

Convergence analysis and numerical validation: Building upon the theoretical convergence analysis presented in Section 3.2, which established that the convergence of the Newton-type solver

is governed by the proper selection of the regularization parameter γ and RBF kernel parameter σ^2 , this section provides an empirical validation of these theoretical findings. The analysis demonstrated that local quadratic convergence is achieved when these parameters are chosen appropriately. The numerical experiments confirm the theoretical predictions. For the representative nonlinear system (Problem 4), the solver exhibits stable residual convergence, typically within 10 to 50 iterations, as depicted in Figure 3). This robust convergence behavior is consistently observed across a wide range of tested problems, with detailed results provided in Appendix B.4 (Table 8). The empirical evidence strongly corroborates the theoretical reliability of the solver for the considered class of problems. Furthermore, the numerical results validate the theoretically indicated parameter configurations. Robust and efficient convergence is achieved with $\gamma = 10^{(6/7)}$ for all sixteen benchmark problems. The kernel parameter is effectively set to $\sigma^2 = 1/8/10$ for first-order ODEs, and $\sigma^2 = 1$ for second-order and higher-order ODEs. See Appendix B.5 for more details. These results collectively demonstrate that the proposed solver delivers numerically stable and efficient convergence across diverse problem types, firmly aligning with the established theoretical framework.

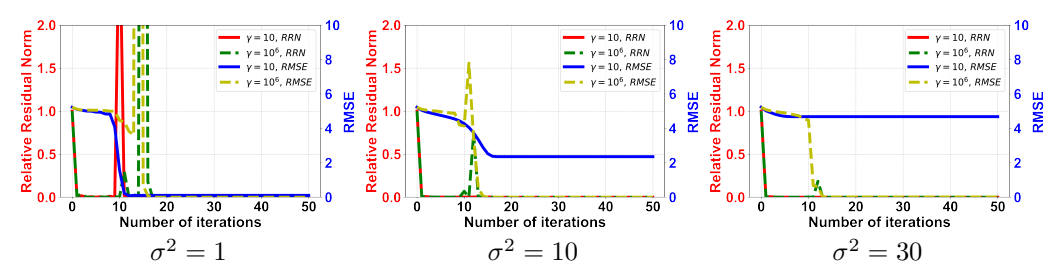


Figure 3: Numerical results of convergence analysis for Problem 4

Comparative analysis with classical numerical methods: RK4 and EAB: To validate the effectiveness of the proposed NLS-SVM method, we conducted a comparative study against two classical numerical techniques: the fourth-order Runge-Kutta method (RK4) and the Explicit Adams-Bashforth (EAB) method. The evaluation was performed on three representative test cases: Problem 3 (stiff ODE). Problem 6 (nonlinear ODE), and Problem 11 (singular

Table 2: Performance comparison for solving Problems 3, 6, and 11 using NLS-SVMs, RK4, and EAB

| ODEs | Model | MAE | RMSE | Train/s | Predict/s |
|------|----------|-----------------------|-----------------------|---------|-----------|
| | NLS-SVMs | 2.06×10 ⁻⁸ | 2.77×10 ⁻⁸ | 0.460 | 0.001 |
| P 3 | RK4 | 3.87×10^{-7} | 3.41×10^{-7} | 0.880 | 0.880 |
| | EAB | 4.97×10^{-8} | 2.90×10^{-8} | 0.030 | 0.030 |
| P 6 | NLS-SVMs | 8.89×10 ⁻⁴ | 1.01×10 ⁻³ | 1.230 | 0.001 |
| FU | RK4 | 1.59×10^{-2} | 1.21×10^{-2} | 0.021 | 0.021 |
| | EAB | 1.28×10^{-6} | 1.11×10^{-6} | 0.036 | 0.036 |
| P 11 | NLS-SVMs | 2.36×10 ⁻⁹ | 2.97×10 ⁻⁹ | 0.100 | 0.001 |
| 1 11 | RK4 | 3.11×10^{-6} | 2.87×10^{-6} | 0.010 | 0.010 |
| | EAB | 1.19×10^{-2} | 6.86×10^{-3} | 0.020 | 0.020 |

ODE). The results are summarized in Table 2. On Problem 3, NLS-SVMs achieved an MAE of 2.06×10^{-8} , which is 18.7 times lower than that of RK4 (3.87×10^{-7}) and 2.4 times lower than that of EAB (4.97×10^{-8}) , while being 880 and 30 times faster in prediction time, respectively. For Problem 6, the proposed method delivered an MAE of 8.89×10^{-4} , reflecting a 17.9-fold improvement over RK4 (1.59×10^{-2}) , along with a 21-fold speedup (0.001 s vs. 0.021 s) in predictions. In the case of the singular ODE (Problem 11), NLS-SVMs maintained high accuracy (MAE= 2.36×10^{-9}), whereas EAB failed with an error nearly 5 million times larger (MAE= 1.19×10^{-2}), establishing the proposed approach as a high-accuracy solver. Additional numerical results are provided in Appendix B.3 (Table 6). It is important to note that the proposed method is not universally superior but offers practical advantages in specific scenarios: (1) it rescues simulations where EAB may fail on singular systems; (2) it enables real-time control applications to stiff systems where RK4 may be computationally prohibitive; (3) it maintains reliability at practical step sizes where other methods require extreme refinement; and (4) it preserves accuracy across a range of step sizes, unlike the step-sensitive errors observed with RK4 and EAB.

Physics-Informed Neural Network Baseline Selection: To establish a rigorous baseline for comparison with the proposed NLS-SVMs method, a systematic model selection procedure was conducted for Physics-Informed Neural Networks (PINNs). The selection process comprised two main stages:

first, an architectural optimization within the Vanilla PINN framework, followed by a comparative evaluation against Fourier Feature PINN to determine the optimal PINN variant. Vanilla PINN Architecture Selection: An ablation study was performed to identify the most effective network architecture for Vanilla PINN. We compared a standard three-layer configuration against an eight-layer architecture using Problem 1 as a benchmark case. The results indicate that the deeper architecture (MAE = 2.32×10^{-3} , RMSE = 2.93×10^{-3} , Time = 1275 s) provides no significant accuracy improvement over the three-layer counterpart (MAE = 4.45×10^{-3} , RMSE = 5.05×10^{-3} , Time = 672s), while incurring a substantial computational overhead (1275 s vs. 672 s). Consequently, the three-layer architecture was selected as it offers the optimal balance between accuracy and efficiency for the class of problems under consideration. This model utilizes identity activation functions, a learning rate of 0.001, and the Adam optimizer, with gradients computed via PyTorch's automatic differentiation. Comparative Evaluation with Fourier Feature PINN: The optimized three-layer Vanilla PINN was then evaluated against Fourier Feature PINN across all 16 benchmark ODEs. Fourier Feature PINN demonstrates superior accuracy in the vast majority of cases. For instance, in Problems 3, 11, and 15, it achieves dramatically lower errors (often by several orders of magnitude) in MAE, RMSE, and L_{∞} norm compared to the Vanilla PINN. Notably, it can also lead to substantially faster training times, as seen in Problems 11 and 15. However, this advantage is not universal. The Vanilla PINN outperforms its counterpart in specific cases like Problems 4, 7, and most notably Problem 16, where the Fourier Feature version fails completely with exceedingly high errors. Furthermore, the Fourier Feature PINN often requires longer computational time, though this is not always the case. Detailed comparison of numerical results are provided in Appendix B.3 (Table 7). Based on this comprehensive analysis, the three-layer Vanilla PINN is selected as the representative PINN baseline for subsequent comparisons with the proposed NLS-SVM method. The chosen model provides a meaningful benchmark for evaluating the relative performance of the proposed method, while Fourier Feature PINN remains recommended for more complex multi-physics or high-gradient scenarios. All subsequent comparisons with PINNs in this study refer to this optimized three-layer Vanilla PINN configuration.

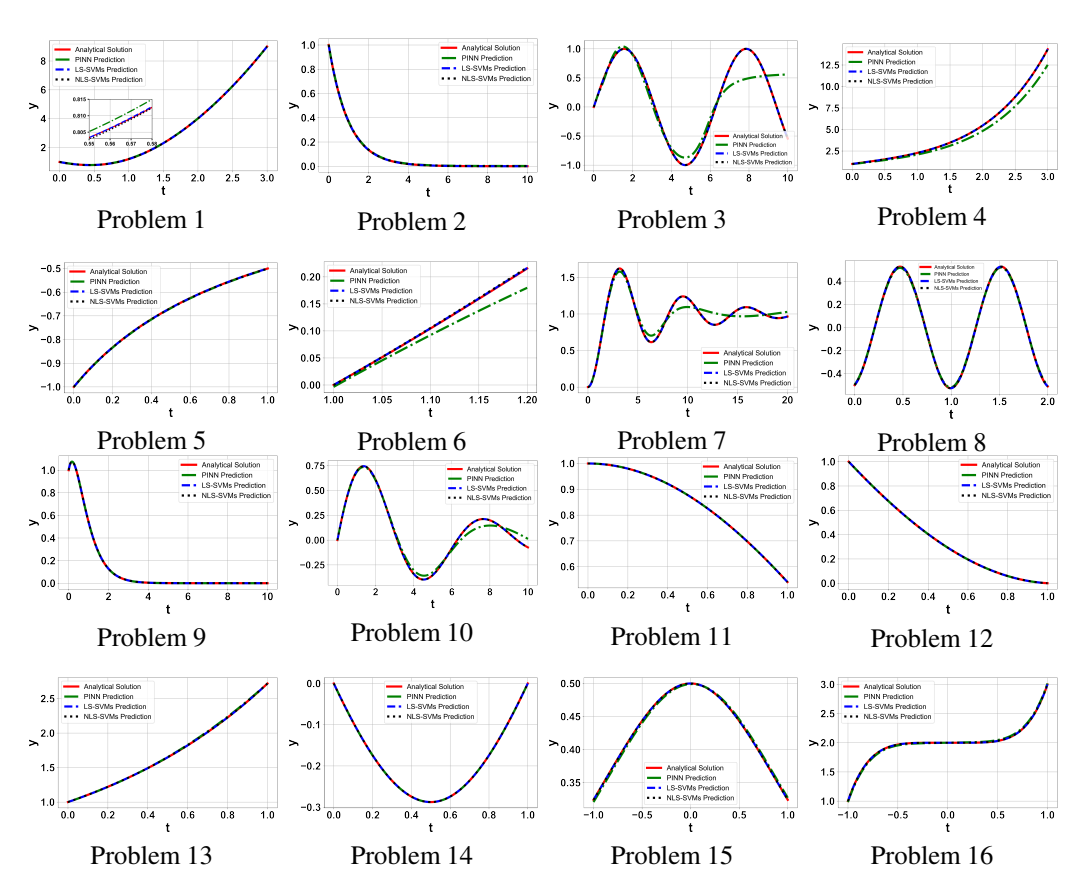


Figure 4: Comparison of model predictions against the analytical solution for Problems 1 to 16

5 Results and discussions

Figure 4 presents the comparision of solutions obtained by LS-SVMs, PINNs, and proposed NLS-SVMs for all 16 benchmark ODEs, with corresponding analytical solutions serving as ground truth. By observation, the proposed NLS-SVMs demonstrate significant improvements in computational efficiency while maintaining competitive solution accuracy relative to classical LS-SVMs. Table 3 quantifies the significant computational speedups (10–6000 times) under comparable accuracy regimes for key benchmarks. Across all test cases, NLS-SVMs achieved comparable solution accuracy to LS-SVMs (< 0.13% relative MAE, RMSE, and $\|y - \hat{y}\|_{\infty}$ difference). Notably, the computational time (including training and prediction time) of NLS-SVMs was reduced by a factor of 10 to 3355 compared to LS-SVMs, depending on the number of time steps n. In comparison to PINNs, the proposed NLS-SVMs model exhibited consistently superior accuracy with maximum reduction by 72% in RMSE, while runs 49-6426 times faster than PINNs (see Appendix B.8 for detailed results).

The scalability of NLS-SVMs is further validated on problems scaled to 100 seconds with $n=5\times10^4$ time steps. Under these large-scale conditions, conventional LS-SVMs and PINNs failed to execute due to memory constraints on the tested hardware, whereas NLS-SVMs produced stable and accurate solutions with execution times between 17.5 and 460 seconds (see Appendix B.6 for details). This performance highlights the method's practical utility in resource-limited settings. While the framework is validated on ODEs, the underlying Nyström acceleration is readily extendable to large-scale partial differential equations by reformulating the differential operators and to other kernel-based ML tasks requiring efficient approximation. It is important to acknowledge a primary limitation of the current method: although it achieves a significant acceleration for nonlinear ODEs, the computational complexity remains at $O(n^3)$. Our future work will focus on breaking this complexity barrier.

Table 3: Comprehensive performance comparison of NLS-SVMs against PINN and LS-SVMs for solving ODEs: accuracy and efficiency

| ODEs | Model | ΔR^2 | $\Delta MAE/\%$ | $\Delta RMSE/\%$ | $\Delta \left\ y - \hat{y} \right\ _{\infty} / \%$ | Speedup |
|------|---|----------------|--|--|--|----------------|
| P4 | NLS-SVMs vs PINN NLS-SVMs vs LS-SVMs | +0.05 +0.00 | $\begin{array}{c} \downarrow 5.34 \times 10^{1} \\ \uparrow 4.94 \times 10^{-2} \end{array}$ | $\begin{array}{c} \downarrow 7.20 \times 10^{1} \\ \uparrow 6.14 \times 10^{-2} \end{array}$ | $\begin{array}{l} \downarrow 1.81 \times 10^2 \\ \uparrow 1.29 \times 10^{-1} \end{array}$ | ↑ 49 ↑ 370 |
| P5 | NLS-SVMs vs PINN NLS-SVMs vs LS-SVMs | -0.00 +0.00 | $\downarrow 1.51 \times 10^{-2}$ $\downarrow 1.00 \times 10^{-3}$ | $\uparrow 3.00 \times 10^{-4} \\ \downarrow 4.00 \times 10^{-3}$ | $\uparrow 5.40 \times 10^{-2}$ $\downarrow 1.70 \times 10^{-2}$ | ↑ 171 ↑ 10 |
| P16 | NLS-SVMs vs PINN NLS-SVMs vs LS-SVMs | +0.00 | $\downarrow 1.24 \times 10^{0}$ $\downarrow 1.33 \times 10^{-2}$ | $\downarrow 1.35 \times 10^{0}$ $\downarrow 1.64 \times 10^{-2}$ | $\downarrow 1.79 \times 10^{0}$ $\downarrow 6.33 \times 10^{-2}$ | ↑ 6426 ↑ 58 |

6 Conclusion

This study introduces a novel Nyström-accelerated Least Squares Support Vector Machines (NLS-SVMs) framework for solving ODEs, establishing a significant improvement in computational efficiency and scalability over classical ML methods such as standard LS-SVMs and physics-informed neural networks (PINNs). The method successfully overcomes the $O(an^3)$ (a=1 for linear ODEs and 27 for nonlinear ODEs) complexity bottleneck inherent in classical LS-SVMs for ODE problems, achieving speedup factors ranging from 10 to 6000—depending on the problem size and characteristics—while consistently preserving solution accuracy. Extensive numerical experiments across 16 benchmark problems confirm the model's versatility and robustness, with relative errors remaining below 0.1% across all tested cases. Even for large-scale systems with fine temporal discretization, the solution time is bounded within 460 seconds, demonstrating the practical viability of the framework in real-time engineering applications such as dynamic system control and multiphysics simulation, where conventional kernel methods or neural models are often limited by memory or latency constraints.

Acknowledgements

The authors acknowledge the funding support provided by the National Natural Science Foundation of China (No. 52208485), the Key Research Project of the Educational Commission of Hubei Province of China (Grant No. D20241203), and the Talent Research Startup Fund of China Three Gorges University (No. 2023RCKJ013).

References

- [1] Edward L Ince. Ordinary differential equations. Courier Corporation, 2012.
- [2] Peter Deuflhard and Folkmar Bornemann. *Scientific computing with ordinary differential equations*, volume 42. Springer Science & Business Media, 2012.
- [3] George D Byrne and Alan C Hindmarsh. Stiff ode solvers: A review of current and coming attractions. *Journal of Computational physics*, 70(1):1–62, 1987.
- [4] Maziar Raissi, Paris Perdikaris, and George E Karniadakis. Physics-informed neural networks: A deep learning framework for solving forward and inverse problems involving nonlinear partial differential equations. *Journal of Computational physics*, 378:686–707, 2019.
- [5] Ricky TQ Chen, Yulia Rubanova, Jesse Bettencourt, and David K Duvenaud. Neural ordinary differential equations. *Advances in neural information processing systems*, 31, 2018.
- [6] Markus Heinonen, Cagatay Yildiz, Henrik Mannerström, Jukka Intosalmi, and Harri Lähdesmäki. Learning unknown ode models with gaussian processes. In *International conference on machine learning*, pages 1959–1968. PMLR, 2018.
- [7] JAK Suykens, T Van Gestel, J De Brabanter, B De Moor, and J Vandewalle. *Least squares support vector machines*. World Scientific Publishing, Singapore, 2002.
- [8] Siamak Mehrkanoon, Tillmann Falck, and Johan AK Suykens. Approximate solutions to ordinary differential equations using least squares support vector machines. *IEEE transactions on neural networks and learning systems*, 23(9):1356–1367, 2012.
- [9] Siamak Mehrkanoon, Saeid Mehrkanoon, and Johan AK Suykens. Parameter estimation of delay differential equations: an integration-free ls-svm approach. *Communications in Nonlinear Science and Numerical Simulation*, 19(4):830–841, 2014.
- [10] Christopher Williams and Matthias Seeger. Using the nyström method to speed up kernel machines. Advances in neural information processing systems, 13, 2000.
- [11] John R Dormand and Peter J Prince. A family of embedded runge-kutta formulae. *Journal of computational and applied mathematics*, 6(1):19–26, 1980.
- [12] Ernst Hairer, Gerhard Wanner, and Syvert P Nørsett. Solving ordinary differential equations I: Nonstiff problems. Springer, 1993.
- [13] Patrick R Conrad, Mark Girolami, Simo Särkkä, Andrew Stuart, and Konstantinos Zygalakis. Statistical analysis of differential equations: introducing probability measures on numerical solutions. *Statistics and Computing*, 27(4):1065–1082, 2017.
- [14] Filip Tronarp, Hans Kersting, Simo Särkkä, and Philipp Hennig. Probabilistic solutions to ordinary differential equations as nonlinear bayesian filtering: a new perspective. *Statistics and Computing*, 29(6):1297–1315, 2019.
- [15] Philipp Hennig, Michael A Osborne, and Hans P Kersting. *Probabilistic Numerics: Computation as Machine Learning*. Cambridge University Press, 2022.
- [16] Nicholas Krämer, Nathanael Bosch, Jonathan Schmidt, and Philipp Hennig. Probabilistic ode solutions in millions of dimensions. In *International Conference on Machine Learning*, pages 11634–11649. PMLR, 2022.
- [17] Jonathan Schmidt, Nicholas Krämer, and Philipp Hennig. A probabilistic state space model for joint inference from differential equations and data. Advances in neural information processing systems, 34:12374–12385, 2021.
- [18] Andrew J Meade Jr and Alvaro A Fernandez. The numerical solution of linear ordinary differential equations by feedforward neural networks. *Mathematical and Computer Modelling*, 19(12):1–25, 1994.

- [19] Hyuk Lee and In Seok Kang. Neural algorithm for solving differential equations. *Journal of computational physics*, 91(1):110–131, 1990.
- [20] Sifan Wang, Yujun Teng, and Paris Perdikaris. Understanding and mitigating gradient flow pathologies in physics-informed neural networks. SIAM Journal on Scientific Computing, 43(5):A3055–A3081, 2021.
- [21] Suyong Kim, Weiqi Ji, Sili Deng, Yingbo Ma, and Christopher Rackauckas. Stiff neural ordinary differential equations. Chaos: An Interdisciplinary Journal of Nonlinear Science, 31(9), 2021.
- [22] Nasim Rahaman, Aristide Baratin, Devansh Arpit, Felix Draxler, Min Lin, Fred Hamprecht, Yoshua Bengio, and Aaron Courville. On the spectral bias of neural networks. In *International* conference on machine learning, pages 5301–5310. PMLR, 2019.
- [23] Amir Gholami, Kurt Keutzer, and George Biros. Anode: unconditionally accurate memory-efficient gradients for neural odes. In *Proceedings of the 28th International Joint Conference on Artificial Intelligence*, pages 730–736, 2019.
- [24] Oliver Hamelijnck, Arno Solin, and Theodoros Damoulas. Physics-informed variational state-space gaussian processes. Advances in Neural Information Processing Systems, 37:98505–98536, 2024.
- [25] Frank Dondelinger, Dirk Husmeier, Simon Rogers, and Maurizio Filippone. Ode parameter inference using adaptive gradient matching with gaussian processes. In *Artificial intelligence and statistics*, pages 216–228. PMLR, 2013.
- [26] NR0960 Aluru. A point collocation method based on reproducing kernel approximations. *International Journal for Numerical Methods in Engineering*, 47(6):1083–1121, 2000.
- [27] Alessandro Rudi, Raffaello Camoriano, and Lorenzo Rosasco. Less is more: Nyström computational regularization. *Advances in neural information processing systems*, 28, 2015.
- [28] Andrea Della Vecchia, Ernesto De Vito, Jaouad Mourtada, and Lorenzo Rosasco. The nyström method for convex loss functions. *Journal of Machine Learning Research*, 25(360):1–60, 2024.
- [29] Petros Drineas and Michael W Mahoney. Randnla: randomized numerical linear algebra. *Communications of the ACM*, 59(6):80–90, 2016.
- [30] Cameron Musco and Christopher Musco. Recursive sampling for the nystrom method. *Advances in neural information processing systems*, 30, 2017.
- [31] Philippe Moireau and Dominique Chapelle. Reduced-order unscented kalman filtering with application parameter identification in large-dimensional systems. *ESAIM: Control, Optimisation and Calculus of Variations*, 17(2):380–405, 2011.
- [32] Carl T Kelley. Iterative methods for linear and nonlinear equations. SIAM, 1995.
- [33] Ron S Dembo, Stanley C Eisenstat, and Trond Steihaug. Inexact newton methods. *SIAM Journal on Numerical analysis*, 19(2):400–408, 1982.
- [34] Stanley C Eisenstat and Homer F Walker. Globally convergent inexact newton methods. *SIAM Journal on Optimization*, 4(2):393–422, 1994.
- [35] Ioannis K Argyros and Saïd Hilout. Weaker conditions for the convergence of newton's method. *Journal of complexity*, 28(3):364–387, 2012.
- [36] Susmita Mall and Snehashish Chakraverty. Comparison of artificial neural network architecture in solving ordinary differential equations. *Advances in Artificial Neural Systems*, 2013(1):181895, 2013.
- [37] Isaac E Lagaris, Aristidis Likas, and Dimitrios I Fotiadis. Artificial neural networks for solving ordinary and partial differential equations. *IEEE transactions on neural networks*, 9(5):987– 1000, 1998.

- [38] Yonghyeon Jeon, Kyung Ryeol Baek, and Sunyoung Bu. Deferred correction neural network techniques for solving ordinary differential equations. *Engineering Applications of Artificial Intelligence*, 135:108771, 2024.
- [39] A Prothero and A Robinson. On the stability and accuracy of one-step methods for solving stiff systems of ordinary differential equations. *Mathematics of Computation*, 28(125):145–162, 1974.
- [40] Ivan Ryzhikov, Eugene Semenkin, and Ilia Panfilov. Evolutionary optimization algorithms for differential equation parameters, initial value and order identification. In *International Conference on Informatics in Control, Automation and Robotics*, volume 2, pages 168–176. SCITEPRESS, 2016.
- [41] Nirmal Kumar, Ali Akbar Shaikh, Sanat Kumar Mahato, and Asoke Kumar Bhunia. Applications of new hybrid algorithm based on advanced cuckoo search and adaptive gaussian quantum behaved particle swarm optimization in solving ordinary differential equations. *Expert Systems with Applications*, 172:114646, 2021.
- [42] Ali Sadollah, Hadi Eskandar, Joong Hoon Kim, et al. Approximate solving of nonlinear ordinary differential equations using least square weight function and metaheuristic algorithms. *Engineering Applications of Artificial Intelligence*, 40:117–132, 2015.
- [43] Luma NM Tawfiq and Ashraf AT Hussein. Design feed forward neural network to solve singular boundary value problems. *International Scholarly Research Notices*, 2013(1):650467, 2013.
- [44] Hongli Sun, Muzhou Hou, Yunlei Yang, Tianle Zhang, Futian Weng, and Feng Han. Solving partial differential equation based on bernstein neural network and extreme learning machine algorithm. *Neural Processing Letters*, 50(2):1153–1172, 2019.
- [45] Shagun Panghal and Manoj Kumar. Optimization free neural network approach for solving ordinary and partial differential equations. *Engineering with Computers*, 37(4):2989–3002, 2021.
- [46] William E Boyce, Richard C DiPrima, and Douglas B Meade. *Elementary differential equations and boundary value problems*. John Wiley & Sons, 2021.
- [47] Endre Süli and David F Mayers. *An introduction to numerical analysis*. Cambridge university press, 2003.
- [48] Alaeddin Malek and R Shekari Beidokhti. Numerical solution for high order differential equations using a hybrid neural network—optimization method. *Applied Mathematics and Computation*, 183(1):260–271, 2006.
- [49] Yanfei Lu, Qingfei Yin, Hongyi Li, Hongli Sun, Yunlei Yang, and Muzhou Hou. The ls-svm algorithms for boundary value problems of high-order ordinary differential equations. *Advances in Difference Equations*, 2019(1):195, 2019.

NeurIPS Paper Checklist

1. Claims

Question: Do the main claims made in the abstract and introduction accurately reflect the paper's contributions and scope?

Answer: [Yes]

Justification: The claims in the abstract and introduction regarding the efficiency and accuracy of our proposed NLS-SVMs are empirically validated by the comprehensive experiments in Section 4. Furthermore, the discussion in Section 5 accurately reflects the scope and limitations of our work.

Guidelines:

- The answer NA means that the abstract and introduction do not include the claims made in the paper.
- The abstract and/or introduction should clearly state the claims made, including the contributions made in the paper and important assumptions and limitations. A No or NA answer to this question will not be perceived well by the reviewers.
- The claims made should match theoretical and experimental results, and reflect how much the results can be expected to generalize to other settings.
- It is fine to include aspirational goals as motivation as long as it is clear that these goals
 are not attained by the paper.

2. Limitations

Question: Does the paper discuss the limitations of the work performed by the authors?

Answer: [Yes]

Justification: See Section 5. It is important to acknowledge a primary limitation of the current method: although it achieves a significant acceleration for nonlinear ODEs, the computational complexity remains at $O(n^3)$.

Guidelines:

- The answer NA means that the paper has no limitation while the answer No means that the paper has limitations, but those are not discussed in the paper.
- The authors are encouraged to create a separate "Limitations" section in their paper.
- The paper should point out any strong assumptions and how robust the results are to violations of these assumptions (e.g., independence assumptions, noiseless settings, model well-specification, asymptotic approximations only holding locally). The authors should reflect on how these assumptions might be violated in practice and what the implications would be.
- The authors should reflect on the scope of the claims made, e.g., if the approach was only tested on a few datasets or with a few runs. In general, empirical results often depend on implicit assumptions, which should be articulated.
- The authors should reflect on the factors that influence the performance of the approach. For example, a facial recognition algorithm may perform poorly when image resolution is low or images are taken in low lighting. Or a speech-to-text system might not be used reliably to provide closed captions for online lectures because it fails to handle technical jargon.
- The authors should discuss the computational efficiency of the proposed algorithms and how they scale with dataset size.
- If applicable, the authors should discuss possible limitations of their approach to address problems of privacy and fairness.
- While the authors might fear that complete honesty about limitations might be used by reviewers as grounds for rejection, a worse outcome might be that reviewers discover limitations that aren't acknowledged in the paper. The authors should use their best judgment and recognize that individual actions in favor of transparency play an important role in developing norms that preserve the integrity of the community. Reviewers will be specifically instructed to not penalize honesty concerning limitations.

3. Theory assumptions and proofs

Question: For each theoretical result, does the paper provide the full set of assumptions and a complete (and correct) proof?

Answer: [Yes]

Justification: Theorem (including proof) and Lemmas are provided in Section 3, and the proofs for Lemmas are provided in Appendices A.4 and A.5.

Guidelines:

- The answer NA means that the paper does not include theoretical results.
- All the theorems, formulas, and proofs in the paper should be numbered and cross-referenced.
- All assumptions should be clearly stated or referenced in the statement of any theorems.
- The proofs can either appear in the main paper or the supplemental material, but if they appear in the supplemental material, the authors are encouraged to provide a short proof sketch to provide intuition.
- Inversely, any informal proof provided in the core of the paper should be complemented by formal proofs provided in appendix or supplemental material.
- Theorems and Lemmas that the proof relies upon should be properly referenced.

4. Experimental result reproducibility

Question: Does the paper fully disclose all the information needed to reproduce the main experimental results of the paper to the extent that it affects the main claims and/or conclusions of the paper (regardless of whether the code and data are provided or not)?

Answer: [Yes]

Justification: Reproducibility notes are present in Appendices A and B.

Guidelines:

- The answer NA means that the paper does not include experiments.
- If the paper includes experiments, a No answer to this question will not be perceived well by the reviewers: Making the paper reproducible is important, regardless of whether the code and data are provided or not.
- If the contribution is a dataset and/or model, the authors should describe the steps taken to make their results reproducible or verifiable.
- Depending on the contribution, reproducibility can be accomplished in various ways. For example, if the contribution is a novel architecture, describing the architecture fully might suffice, or if the contribution is a specific model and empirical evaluation, it may be necessary to either make it possible for others to replicate the model with the same dataset, or provide access to the model. In general, releasing code and data is often one good way to accomplish this, but reproducibility can also be provided via detailed instructions for how to replicate the results, access to a hosted model (e.g., in the case of a large language model), releasing of a model checkpoint, or other means that are appropriate to the research performed.
- While NeurIPS does not require releasing code, the conference does require all submissions to provide some reasonable avenue for reproducibility, which may depend on the nature of the contribution. For example
 - (a) If the contribution is primarily a new algorithm, the paper should make it clear how to reproduce that algorithm.
- (b) If the contribution is primarily a new model architecture, the paper should describe the architecture clearly and fully.
- (c) If the contribution is a new model (e.g., a large language model), then there should either be a way to access this model for reproducing the results or a way to reproduce the model (e.g., with an open-source dataset or instructions for how to construct the dataset).
- (d) We recognize that reproducibility may be tricky in some cases, in which case authors are welcome to describe the particular way they provide for reproducibility. In the case of closed-source models, it may be that access to the model is limited in some way (e.g., to registered users), but it should be possible for other researchers to have some path to reproducing or verifying the results.

5. Open access to data and code

Question: Does the paper provide open access to the data and code, with sufficient instructions to faithfully reproduce the main experimental results, as described in supplemental material?

Answer: [Yes]

Justification: The python code implementing the proposed NLS-SVMs method is available at https://github.com/AI4SciCompLab/NLS-SVMs.

Guidelines:

- The answer NA means that paper does not include experiments requiring code.
- Please see the NeurIPS code and data submission guidelines (https://nips.cc/public/guides/CodeSubmissionPolicy) for more details.
- While we encourage the release of code and data, we understand that this might not be possible, so "No" is an acceptable answer. Papers cannot be rejected simply for not including code, unless this is central to the contribution (e.g., for a new open-source benchmark).
- The instructions should contain the exact command and environment needed to run to reproduce the results. See the NeurIPS code and data submission guidelines (https://nips.cc/public/guides/CodeSubmissionPolicy) for more details.
- The authors should provide instructions on data access and preparation, including how to access the raw data, preprocessed data, intermediate data, and generated data, etc.
- The authors should provide scripts to reproduce all experimental results for the new proposed method and baselines. If only a subset of experiments are reproducible, they should state which ones are omitted from the script and why.
- At submission time, to preserve anonymity, the authors should release anonymized versions (if applicable).
- Providing as much information as possible in supplemental material (appended to the paper) is recommended, but including URLs to data and code is permitted.

6. Experimental setting/details

Question: Does the paper specify all the training and test details (e.g., data splits, hyperparameters, how they were chosen, type of optimizer, etc.) necessary to understand the results?

Answer: [Yes]

Justification: See Section 4 and Appendix B.

Guidelines:

- The answer NA means that the paper does not include experiments.
- The experimental setting should be presented in the core of the paper to a level of detail that is necessary to appreciate the results and make sense of them.
- The full details can be provided either with the code, in appendix, or as supplemental
 material.

7. Experiment statistical significance

Question: Does the paper report error bars suitably and correctly defined or other appropriate information about the statistical significance of the experiments?

Answer: [Yes]

Justification: We visualize our experimental results with informative figures and tables. These include key metrics like \mathbb{R}^2 , RMSE, and MAE.

Guidelines:

- The answer NA means that the paper does not include experiments.
- The authors should answer "Yes" if the results are accompanied by error bars, confidence intervals, or statistical significance tests, at least for the experiments that support the main claims of the paper.

- The factors of variability that the error bars are capturing should be clearly stated (for example, train/test split, initialization, random drawing of some parameter, or overall run with given experimental conditions).
- The method for calculating the error bars should be explained (closed form formula, call to a library function, bootstrap, etc.)
- The assumptions made should be given (e.g., Normally distributed errors).
- It should be clear whether the error bar is the standard deviation or the standard error
 of the mean.
- It is OK to report 1-sigma error bars, but one should state it. The authors should preferably report a 2-sigma error bar than state that they have a 96% CI, if the hypothesis of Normality of errors is not verified.
- For asymmetric distributions, the authors should be careful not to show in tables or figures symmetric error bars that would yield results that are out of range (e.g. negative error rates).
- If error bars are reported in tables or plots, The authors should explain in the text how they were calculated and reference the corresponding figures or tables in the text.

8. Experiments compute resources

Question: For each experiment, does the paper provide sufficient information on the computer resources (type of compute workers, memory, time of execution) needed to reproduce the experiments?

Answer: [Yes]

Justification: See Section 4. All numerical experiments in this study were conducted on a computer system equipped with an Intel(R) Core(TM) i9-14900HX processor, 32 GB of RAM.

Guidelines:

- The answer NA means that the paper does not include experiments.
- The paper should indicate the type of compute workers CPU or GPU, internal cluster, or cloud provider, including relevant memory and storage.
- The paper should provide the amount of compute required for each of the individual experimental runs as well as estimate the total compute.
- The paper should disclose whether the full research project required more compute than the experiments reported in the paper (e.g., preliminary or failed experiments that didn't make it into the paper).

9. Code of ethics

Question: Does the research conducted in the paper conform, in every respect, with the NeurIPS Code of Ethics https://neurips.cc/public/EthicsGuidelines?

Answer: [Yes]

Justification: The research conducted in the paper conform, in every respect, with the NeurIPS Code of Ethics.

Guidelines:

- The answer NA means that the authors have not reviewed the NeurIPS Code of Ethics.
- If the authors answer No, they should explain the special circumstances that require a
 deviation from the Code of Ethics.
- The authors should make sure to preserve anonymity (e.g., if there is a special consideration due to laws or regulations in their jurisdiction).

10. Broader impacts

Question: Does the paper discuss both potential positive societal impacts and negative societal impacts of the work performed?

Answer: [Yes]

Justification: Potential positive impacts include accelerating scientific discovery and engineering design, as discussed in Sections 5 and 6.

Guidelines:

- The answer NA means that there is no societal impact of the work performed.
- If the authors answer NA or No, they should explain why their work has no societal
 impact or why the paper does not address societal impact.
- Examples of negative societal impacts include potential malicious or unintended uses (e.g., disinformation, generating fake profiles, surveillance), fairness considerations (e.g., deployment of technologies that could make decisions that unfairly impact specific groups), privacy considerations, and security considerations.
- The conference expects that many papers will be foundational research and not tied to particular applications, let alone deployments. However, if there is a direct path to any negative applications, the authors should point it out. For example, it is legitimate to point out that an improvement in the quality of generative models could be used to generate deepfakes for disinformation. On the other hand, it is not needed to point out that a generic algorithm for optimizing neural networks could enable people to train models that generate Deepfakes faster.
- The authors should consider possible harms that could arise when the technology is being used as intended and functioning correctly, harms that could arise when the technology is being used as intended but gives incorrect results, and harms following from (intentional or unintentional) misuse of the technology.
- If there are negative societal impacts, the authors could also discuss possible mitigation strategies (e.g., gated release of models, providing defenses in addition to attacks, mechanisms for monitoring misuse, mechanisms to monitor how a system learns from feedback over time, improving the efficiency and accessibility of ML).

11. Safeguards

Question: Does the paper describe safeguards that have been put in place for responsible release of data or models that have a high risk for misuse (e.g., pretrained language models, image generators, or scraped datasets)?

Answer: [NA]

Justification: The answer NA means that the paper poses no such risks.

Guidelines:

- The answer NA means that the paper poses no such risks.
- Released models that have a high risk for misuse or dual-use should be released with necessary safeguards to allow for controlled use of the model, for example by requiring that users adhere to usage guidelines or restrictions to access the model or implementing safety filters.
- Datasets that have been scraped from the Internet could pose safety risks. The authors should describe how they avoided releasing unsafe images.
- We recognize that providing effective safeguards is challenging, and many papers do
 not require this, but we encourage authors to take this into account and make a best
 faith effort.

12. Licenses for existing assets

Question: Are the creators or original owners of assets (e.g., code, data, models), used in the paper, properly credited and are the license and terms of use explicitly mentioned and properly respected?

Answer: [Yes]

Justification: The source code implemented in this study is proprietary and developed entirely by the authors. No external assets such as third-party code, data, or pre-trained models were used. Therefore, all materials are appropriately credited and utilized in accordance with their original terms.

Guidelines:

- The answer NA means that the paper does not use existing assets.
- The authors should cite the original paper that produced the code package or dataset.

- The authors should state which version of the asset is used and, if possible, include a URL.
- The name of the license (e.g., CC-BY 4.0) should be included for each asset.
- For scraped data from a particular source (e.g., website), the copyright and terms of service of that source should be provided.
- If assets are released, the license, copyright information, and terms of use in the package should be provided. For popular datasets, paperswithcode.com/datasets has curated licenses for some datasets. Their licensing guide can help determine the license of a dataset.
- · For existing datasets that are re-packaged, both the original license and the license of the derived asset (if it has changed) should be provided.
- If this information is not available online, the authors are encouraged to reach out to the asset's creators.

13. New assets

Question: Are new assets introduced in the paper well documented and is the documentation provided alongside the assets?

Answer: [Yes]

Justification: Full documentation is provided to ensure the complete reproducibility of our work. All newly introduced code is well-documented and accompanied by usage examples.

Guidelines:

- The answer NA means that the paper does not release new assets.
- · Researchers should communicate the details of the dataset/code/model as part of their submissions via structured templates. This includes details about training, license, limitations, etc.
- The paper should discuss whether and how consent was obtained from people whose asset is used.
- At submission time, remember to anonymize your assets (if applicable). You can either create an anonymized URL or include an anonymized zip file.

14. Crowdsourcing and research with human subjects

Question: For crowdsourcing experiments and research with human subjects, does the paper include the full text of instructions given to participants and screenshots, if applicable, as well as details about compensation (if any)?

Answer: [NA]

Justification: The answer NA means that the paper does not involve crowdsourcing nor research with human subjects.

Guidelines:

- The answer NA means that the paper does not involve crowdsourcing nor research with human subjects.
- Including this information in the supplemental material is fine, but if the main contribution of the paper involves human subjects, then as much detail as possible should be included in the main paper.
- According to the NeurIPS Code of Ethics, workers involved in data collection, curation, or other labor should be paid at least the minimum wage in the country of the data collector.

15. Institutional review board (IRB) approvals or equivalent for research with human subjects

Ouestion: Does the paper describe potential risks incurred by study participants, whether such risks were disclosed to the subjects, and whether Institutional Review Board (IRB) approvals (or an equivalent approval/review based on the requirements of your country or institution) were obtained?

Answer: [NA]

Justification: The answer NA means that the paper does not involve crowdsourcing nor research with human subjects.

Guidelines:

- The answer NA means that the paper does not involve crowdsourcing nor research with human subjects.
- Depending on the country in which research is conducted, IRB approval (or equivalent) may be required for any human subjects research. If you obtained IRB approval, you should clearly state this in the paper.
- We recognize that the procedures for this may vary significantly between institutions and locations, and we expect authors to adhere to the NeurIPS Code of Ethics and the guidelines for their institution.
- For initial submissions, do not include any information that would break anonymity (if applicable), such as the institution conducting the review.

16. Declaration of LLM usage

Question: Does the paper describe the usage of LLMs if it is an important, original, or non-standard component of the core methods in this research? Note that if the LLM is used only for writing, editing, or formatting purposes and does not impact the core methodology, scientific rigorousness, or originality of the research, declaration is not required.

Answer: [NA]

Justification: The answer NA means that the core method development in this research does not involve LLMs as any important, original, or non-standard components.

Guidelines:

- The answer NA means that the core method development in this research does not involve LLMs as any important, original, or non-standard components.
- Please refer to our LLM policy (https://neurips.cc/Conferences/2025/LLM) for what should or should not be described.

A Technical Appendices

A.1 Least Squares Support Vector Machines (LS-SVMs)

The learning objective of LS-SVMs is to find a nonlinear mapping relationship [7] between the input variable $x_i \in R^d$ and the output variable $y_i \in R$ from the given training dataset $\{x_i, y_i\}_{i=1}^n$. The goal in a regression problem is to estimate a model of the form $y(x) = \omega^T \varphi(x) + b$. A simple description of the mathematical model follows:

$$\underset{\boldsymbol{\omega}, b, e_i}{\text{minimize}} : J_p\left(\boldsymbol{\omega}, e_i\right) = \frac{1}{2}\boldsymbol{\omega}^T \boldsymbol{\omega} + \frac{\gamma}{2} \sum_{i=1}^n e_i^2$$
(22)

subject to :
$$y_i = \boldsymbol{\omega}^T \boldsymbol{\varphi}(\boldsymbol{x}_i) + b + e_i, \qquad i = 1, ..., n$$
 (23)

where $e_i \in R$ denotes the error variable, γ is a regularization parameter, $b \in R$ is the bias term, $\omega \in R^h$ is the weight parameters, $\varphi(\boldsymbol{x}_i) \in R^h$ is a high-dimensional feature variable of input data \boldsymbol{x}_i , where $\varphi(\cdot): R^d \to R^h$ is the feature map and h is the dimension of the feature space, and y_i indicates the output data. The dual solution is then given by

$$\left[\begin{array}{c|c} \mathbf{\Omega} + \mathbf{I}_{n \times n} / \gamma & \mathbf{1}_n \\ \mathbf{1}_n^T & 0 \end{array} \right] \left[\begin{array}{c} \boldsymbol{\alpha} \\ \overline{b} \end{array} \right] = \left[\begin{array}{c} \boldsymbol{y} \\ \overline{0} \end{array} \right]$$
(24)

where $\Omega_{ij} = K(\boldsymbol{x}_i, \boldsymbol{x}_j) = \boldsymbol{\varphi}(\boldsymbol{x}_i)^T \boldsymbol{\varphi}(\boldsymbol{x}_j)$ is the ij-th entry of the kernel matrix. $\mathbf{1}_n = [1, \dots, 1]^T \in \mathbb{R}^n$, $\boldsymbol{\alpha} = [\alpha_1, \dots, \alpha_n]^T$, $\mathbf{y} = [y_1, \dots, y_n]^T$ and $\mathbf{I}_{n \times n}$ is the identity matrix. The model in the dual form becomes: $y(\boldsymbol{x}) = \sum_{i=1}^n \alpha_i K(\boldsymbol{x}, \boldsymbol{x}_i) + b$.

A.2 LS-SVM for p-th order nonlinear ODE

The Lagrangian of the constrained optimization problem becomes

$$\mathcal{L}(\boldsymbol{\omega}, b, e_{i}, \xi_{i}, y_{i}, \alpha_{i}, \eta_{i}, \beta_{i}) = \frac{1}{2} \boldsymbol{\omega}^{T} \boldsymbol{\omega} + \frac{\gamma}{2} \sum_{i=1}^{n} e_{i}^{2} + \frac{\gamma}{2} \sum_{i=1}^{n} \xi_{i}^{2}$$

$$- \sum_{i=2}^{N} \alpha_{i} \left(\boldsymbol{\omega}^{T} \boldsymbol{\varphi}^{(p)}(t_{i}) - f\left(t_{i}, y_{t_{i}}^{(p-1)}, ..., y_{t_{i}}^{\prime}, y_{t_{i}}\right) - e_{i} \right)$$

$$- \beta_{1} \left(\boldsymbol{\omega}^{T} \boldsymbol{\varphi}(t_{1}) + b - v_{1} \right) - ... - \beta_{p} \left(\boldsymbol{\omega}^{T} \boldsymbol{\varphi}^{(p-1)}(t_{1}) - v_{p} \right)$$

$$- \sum_{i=2}^{N} \eta_{i} \left(y_{i} - \boldsymbol{\omega}^{T} \boldsymbol{\varphi}(t_{i}) - b - \xi_{i} \right)$$

$$(25)$$

After obtaining KKT optimality conditions and making use of Mercer's theorem, the solution is obtained in the dual by solving the following nonlinear system of equations:

| $\widehat{m{\Omega}_1^1}$ | $	ilde{m{\Omega}}_0^1$ | $oldsymbol{h}_{1}^{T}$ | 0_{n-1} | $0_{(n-1)\times(n-1)}$ |] | α | | f(y) | |
|--------------------------------------|---------------------------|---|---------------|------------------------|-----|-------------------------------------|---|---|------|
| $\left(ilde{m{\Omega}}_0^1 ight)^T$ | $\widehat{m{\Omega}}_0^0$ | $oldsymbol{h}_0^T$ | 1_{n-1} | $-I_{n-1}$ | | $\frac{\boldsymbol{\eta}}{\beta_1}$ | | $\frac{0_{n-1}}{v_1}$ | |
| h_1 | h_0 | $\left[\left[oldsymbol{\Omega}_{0}^{0} ight]_{1,1}$ | 1 | 0_{n-1}^T | | | = | | (26) |
| | | | | | Ш | β_{p-1} | | v_{p-1} | |
| 0_{n-1}^T | 1_{n-1}^{T} | 1 | 0 | 0_{n-1}^T | | <u>b</u> | | $\frac{0}{2}$ | |
| D(y) | I_{n-1} | ${\bf 0}_{n-1}$ | 0_{n-1} | $0_{(n-1)\times(n-1)}$ | ا ا | $oxed{y}$ | I | $\begin{bmatrix} 0_{n-1} \end{bmatrix}$ | |

where

$$\begin{split} &\widehat{\boldsymbol{\Omega}}_{1}^{1} = \widetilde{\boldsymbol{\Omega}}_{1}^{1} + I_{n-1}/\gamma, \quad \widehat{\boldsymbol{\Omega}}_{0}^{0} = \widetilde{\boldsymbol{\Omega}}_{0}^{0} + I_{n-1}/\gamma, D(\boldsymbol{y}) = \operatorname{diag}\left(f'(\boldsymbol{y})\right) \\ &\boldsymbol{f}(\boldsymbol{y}) = \left[f\left(t_{2}, y_{2}\right), \dots, f\left(t_{n}, y_{n}\right)\right]^{T}, \boldsymbol{f}'(\boldsymbol{y}) = \left[\left.\frac{\partial f(t, y)}{\partial y}\right|_{t=t_{2}, y=y_{2}}, \dots, \left.\frac{\partial f(t, y)}{\partial y}\right|_{t=t_{n}, y=y_{n}}\right] \\ &\boldsymbol{\alpha} = \left[\alpha_{2}, \dots, \alpha_{n}\right]^{T}, \boldsymbol{\eta} = \left[\eta_{2}, \dots, \eta_{n}\right]^{T}, \boldsymbol{y} = \left[y_{2}, \dots, y_{n}\right]^{T}, \widetilde{\boldsymbol{\Omega}}_{0}^{0} = \left[\boldsymbol{\Omega}_{0}^{0}\right]_{2:n, 2:n} \\ &\widetilde{\boldsymbol{\Omega}}_{1}^{1} = \left[\boldsymbol{\Omega}_{1}^{1}\right]_{2:n, 2:n}, \widetilde{\boldsymbol{\Omega}}_{0}^{1} = \left[\boldsymbol{\Omega}_{0}^{1}\right]_{2:n, 2:n}, \boldsymbol{h}_{\boldsymbol{0}} = \left[\left[\boldsymbol{\Omega}_{0}^{0}\right]_{1, 2}, \dots, \left[\boldsymbol{\Omega}_{0}^{0}\right]_{1, n}\right] \\ &\boldsymbol{h}_{1} = \left[\left[\boldsymbol{\Omega}_{0}^{1}\right]_{1, 2}, \dots, \left[\boldsymbol{\Omega}_{0}^{1}\right]_{1, n}\right], \boldsymbol{0}_{n-1} = \left[0, \dots, 0\right]^{T} \in \mathbb{R}^{n-1} \end{split}$$

A.3 Nyström Method for Feature Formulation

This appendix section presents the nonlinear feature mapping using Nyström method [7] . Firstly, given the input dataset $\{t_i\}_{i=1}^n$, the corresponding kernel matrix consisting of Gaussian kernel functions is denoted as $\Omega(n,n) \in R^{n\times n}$, where $\Omega_{i,j} = K(t_i,t_j), i,j=1,...,n$. According to Mercer's theorem, in a high-dimensional $h(n < h \leq \infty)$ feature space, the following relation can be obtained:

$$K(t_i, t_j) = \sum_{k=1}^{h} \varsigma_k \phi_k(t_i) \phi_k(t_j)$$
(27)

where $\zeta_1 \geq \zeta_2 \geq \cdots \geq 0$ represent the eigenvalues; $\phi_1, \phi_2, \cdots, \phi_h$ represent the corresponding eigenfunctions. The eigenvalues and eigenfunctions are associated with the following integral equation:

$$\int K(\boldsymbol{z}, \boldsymbol{t}) \phi_k(t) p(t) dt = \varsigma_k \phi_k(\boldsymbol{z})$$
(28)

where p(t) represents the continuous-type probability density function of the input space t. In case of a large-scale training dataset $\{t_i, y_i\}_{i=1}^n$, it is assumed that the input space $\{t_i\}_{i=1}^n$ is distributed independently and identically between them, and all of them are sampled from p(t). To approximate the integral equation of the above eigenfunction, m sample data $\{t_s, y_s\}_{s=1}^m (m \ll n)$ can be selected from the large-scale training dataset $\{t_i, y_i\}_{i=1}^n$, In this case, p(t) can be approximated by the sampled input dataset $\{t_s\}_{s=1}^m$ so that the continuous p(t) can be characterized by the discrete $\{t_s\}_{s=1}^m$. Then, Eq.(28) can be written as follows:

$$\frac{1}{m} \sum_{s=1}^{m} K(\boldsymbol{z}, t_s) \phi_k(t_s) \approx \varsigma_k \phi_k(\boldsymbol{z})$$
 (29)

For the selected sample data $\{t_s\}_{s=1}^m$, the corresponding kernel matrix $\Omega(m, m)$ and the decomposition of its eigenvalues and eigenvectors can be described by the following relation:

$$\mathbf{\Omega}_{(m,m)}\hat{\mathbf{\Phi}}_{(m\times m)} = \hat{\mathbf{\Phi}}_{(m\times m)}\hat{\mathbf{\Lambda}}_{(m\times m)} \tag{30}$$

where $\Omega_{(m,m)} \in R^{m imes m}$ represents the small-scale kernel matrix approximating the large-scale original kernel matrix $\Omega_{(n,n)}$ by $\Omega_{(n,n)} \cong \Omega_{(n,m)} [\Omega_{(m,m)}]^{-1} \Omega_{(m,n)}$ with elements $\Omega_{sz} = K(t_s,t_z)$, s,z=1,...,m; $\hat{\Phi}_{(m imes m)} \in R^{m imes m}$ represents a matrix consisting of the eigenvectors of the kernel matrix $\Omega_{(m,m)}$, where $\hat{\Phi}_{sk} = \hat{\phi}_k(t_s), s, k=1,...,m$, and $\hat{\Lambda}_{(m imes m)} = diag([\hat{\varsigma}_1;...;\hat{\varsigma}_m]) \in R^{m imes m}$ represents the diagonal matrix consisting of the eigenvalues of the kernel matrix $\Omega_{(m,m)}$. Since $\Omega_{(m,m)}$ is a symmetric semi-positive definite matrix, each element in $\hat{\Lambda}_{(m imes m)}$ is no less than 0.

Then we can utilize the eigenvalues and eigenvectors of the small-scale kernel matrix $\mathbf{Q} = \mathbf{\Omega}_{(m,m)}$ to extract the features based on the proposed NLS-SVMs. By replacing \mathbf{z} in Eq.(29) with t_z and substituting s, z, k = 1, ..., q all into Eq.(29) and writing the summary equation in the form of Eq.(30), the following equation is derived:

$$\phi_k(t_s) \approx \sqrt{m}\hat{\Phi}_{sk}; \qquad \varsigma_k = \frac{1}{m}\hat{\varsigma}_k$$
 (31)

Substituting Eq.(31) into Eq.(29) leads to the k-th eigenfunction expression:

$$\phi_k(\boldsymbol{t_z}) \approx \frac{\sqrt{m}}{\hat{\varsigma}_k} \sum_{s=1}^m K(t_z, t_s) \hat{\Phi}_{sk}$$
 (32)

The relation between the high-dimensional vector $\varphi(t_i)$ and the eigenfunction $\phi(t_i)$ can be derived as follows:

$$\varphi^{T}(t_{i})\varphi(t_{j}) = \sum_{k=1}^{m} \sqrt{\hat{\varsigma}_{k}} \phi_{k}(t_{i}) \sqrt{\hat{\varsigma}_{k}} \phi_{k}(t_{j})$$
(33)

Since $\varphi^T(t_i)\varphi(t_j) = \sum_{k=1}^q \varphi_k(t_i)\varphi_k(t_j)$, substituting this into Eq.(32) and combining it with Eq.(31), we get the following:

$$\varphi_k(t_i) = \sqrt{\hat{\varsigma}_k} \phi_k(t_i) = \frac{\sqrt{m}}{\sqrt{\hat{\varsigma}_k}} \sum_{k=1}^m \hat{\Phi}_{sk} K(t_k, t_i)$$
(34)

The high-dimensional feature vector $\varphi(t_i) \in R^m \ (m \ll n)$ can be obtained from Eq.(34), where $\varphi(t_i) = [\varphi_1(t_i), ..., \varphi_m(t_i)]^T$.

A.4 NLS-SVMs for Lemma 1

Proof 1: The constraint conditions include n time-discrete equations where each represents the discretized form of the ODE equation itself at each time point. The Lagrangian of the constrained optimization problem (Eq.(9)) becomes:

$$L(\boldsymbol{\omega}, b, \lambda_{1}, ..., \lambda_{p}) = \frac{1}{2} \boldsymbol{\omega}^{T} \boldsymbol{\omega} + \frac{\gamma}{2} \left(\boldsymbol{\omega}^{T} \boldsymbol{\varphi}^{(p)} \left(t_{i} \right) - \left(\boldsymbol{\omega}^{T} \left[\sum_{k=1}^{p} \boldsymbol{f}_{k} \left(t_{i} \right) \boldsymbol{\varphi}_{i}^{(p-k)} \right] + \boldsymbol{f}_{p} \left(t_{i} \right) \boldsymbol{b} + r \left(t_{i} \right) \right) \right)^{T}$$

$$\left(\boldsymbol{\omega}^{T} \boldsymbol{\varphi}^{(p)} \left(t_{i} \right) - \left(\boldsymbol{\omega}^{T} \left[\sum_{k=1}^{p} \boldsymbol{f}_{k} \left(t_{i} \right) \boldsymbol{\varphi}_{i}^{(p-k)} \right] + f_{p} \left(t_{i} \right) \boldsymbol{b} + r \left(t_{i} \right) \right) \right)$$

$$+ \lambda_{1} \left(\boldsymbol{\omega}^{T} \boldsymbol{\varphi}(t_{1}) + \boldsymbol{b} - v_{1} \right)$$

$$+ ... + \lambda_{p} \left(\boldsymbol{\omega}^{T} \boldsymbol{\varphi}^{(p-1)} \left(t_{1} \right) - v_{p} \right)$$

$$(35)$$

Then the Karush–Kuhn–Tucker (KKT) optimality conditions are as follows:

$$\begin{cases}
\frac{\partial L(\boldsymbol{\omega}, b, \lambda_{1}, \dots, \lambda_{p})}{\partial \boldsymbol{\omega}} = \left[\boldsymbol{E} + \mathbf{A} \left(\boldsymbol{\Psi}^{(p)} - \boldsymbol{f}_{1} \boldsymbol{\Psi}^{(p-1)} - \dots - \boldsymbol{f}_{p} \boldsymbol{\Psi} \right) \right] \boldsymbol{\omega} \\
- \left[\mathbf{A} \left(\boldsymbol{f}_{p} \cdot \mathbf{1} \right) \right] b + \boldsymbol{\varphi}^{T} (t_{1}) \lambda_{1} + \dots + \left(\boldsymbol{\varphi}^{(p-1)} (t_{1}) \right)^{T} \lambda_{p} - \mathbf{A} \boldsymbol{r}
\end{cases}$$

$$\frac{\partial L(\boldsymbol{\omega}, b, \lambda_{1}, \dots, \lambda_{p})}{\partial b} = \left[\boldsymbol{V} \left(\boldsymbol{\Psi}^{(p)} - \boldsymbol{f}_{1} \boldsymbol{\Psi}^{(p-1)} - \dots - \boldsymbol{f}_{p} \boldsymbol{\Psi} \right) \right] \boldsymbol{\omega} \\
- \left[\boldsymbol{V} \left(\boldsymbol{f}_{p} \cdot \mathbf{1} \right) \right] b + \lambda_{1} - \boldsymbol{V} \boldsymbol{r}
\end{cases}$$

$$\frac{\partial L(\boldsymbol{\omega}, b, \lambda_{1}, \dots, \lambda_{p})}{\partial \lambda_{1}} = \boldsymbol{\varphi}(t_{1})^{T} \boldsymbol{\omega} + b - v_{1}$$

$$\vdots$$

$$\frac{\partial L(\boldsymbol{\omega}, b, \lambda_{1}, \dots, \lambda_{p})}{\partial \lambda_{p}} = \left(\boldsymbol{\varphi}^{(p-1)} (t_{1}) \right)^{T} \boldsymbol{\omega} - v_{p}$$
(36)

Therefore, these equations in the matrix from gives the linear system in Eq.(10). The model in the primal problem: $\hat{y}(t) = \omega^T \varphi(t) + b$

A.5 Nyström Method for Lemma 2

Proof 2: The Lagrangian of the constrained optimization problem Eq.(4) in its primal form becomes:

$$L(\boldsymbol{\omega}, b, \lambda_1, ... \lambda_p, \boldsymbol{y}_i) = \frac{1}{2} \boldsymbol{\omega}^T \boldsymbol{\omega} + \frac{\gamma}{2} \left(\boldsymbol{\omega}^T \boldsymbol{\varphi}^{(p)}(t_i) - f(t_i, y_{t_i}^{(p-1)}, ..., y_{t_i}', y_{t_i}) \right)^T$$

$$\left(\boldsymbol{\omega}^T \boldsymbol{\varphi}^{(p)}(t_i) - f(t_i, y_{t_i}^{(p-1)}, ..., y_{t_i}', y_{t_i}) \right) + \frac{\gamma}{2} \left(\boldsymbol{y}_{t_i} - \boldsymbol{\omega}^T \boldsymbol{\varphi}(t_i) - b \right)^T$$

$$\left(\boldsymbol{y}_{t_i} - \boldsymbol{\omega}^T \boldsymbol{\varphi}(t_i) - b \right) + \lambda_p \left(\boldsymbol{\omega}^T \boldsymbol{\varphi}^{(p)}(t_1) - v_p \right)$$

$$+ ... + \lambda_1 \left(\boldsymbol{\omega}^T \boldsymbol{\varphi}(t_1) + b - v_1 \right)$$

$$(37)$$

Then the KKT optimality conditions are as follows:

$$\begin{cases}
\frac{\partial L(\boldsymbol{\omega}, b, \lambda_{1}, \dots, \lambda_{p}, \boldsymbol{y}_{i})}{\partial \boldsymbol{\omega}} = \boldsymbol{Y}_{1} \stackrel{Jacobian}{\rightarrow} \frac{\partial \boldsymbol{Y}_{1}}{\partial (\boldsymbol{\omega}, b, \lambda_{1}, \dots, \lambda_{p}, \boldsymbol{y}_{i})} \\
\frac{\partial L(\boldsymbol{\omega}, b, \lambda_{1}, \dots, \lambda_{p}, \boldsymbol{y}_{i})}{\partial b} = Y_{2} \stackrel{Jacobian}{\rightarrow} \frac{\partial Y_{2}}{\partial (\boldsymbol{\omega}, b, \lambda_{1}, \dots, \lambda_{p}, \boldsymbol{y}_{i})} \\
\frac{\partial L(\boldsymbol{\omega}, b, \lambda_{1}, \dots, \lambda_{p}, \boldsymbol{y}_{i})}{\partial \lambda_{1}} = Y_{3} \stackrel{Jacobian}{\rightarrow} \frac{\partial Y_{3}}{\partial (\boldsymbol{\omega}, b, \lambda_{1}, \dots, \lambda_{p}, \boldsymbol{y}_{i})} \\
\vdots \\
\frac{\partial L(\boldsymbol{\omega}, b, \lambda_{1}, \dots, \lambda_{p}, \boldsymbol{y}_{i})}{\partial \lambda_{p}} = Y_{p+2} \stackrel{Jacobian}{\rightarrow} \frac{\partial Y_{p+2}}{\partial (\boldsymbol{\omega}, b, \lambda_{1}, \dots, \lambda_{p}, \boldsymbol{y}_{i})} \\
\frac{\partial L(\boldsymbol{\omega}, b, \lambda_{1}, \dots, \lambda_{p}, \boldsymbol{y}_{i})}{\partial \boldsymbol{y}_{i}} = \boldsymbol{Y}_{p+3} \stackrel{Jacobian}{\rightarrow} \frac{\partial \boldsymbol{Y}_{p+2}}{\partial (\boldsymbol{\omega}, b, \lambda_{1}, \dots, \lambda_{p}, \boldsymbol{y}_{i})}
\end{cases}$$
(38)

Therefore, these equations in the matrix from gives the nonlinear system in Eq.(11). The model in the primal form becomes $\hat{y}(t) = \omega^T \varphi(t) + b$.

A.6 NLS-SVMs for Solving First-Order ODE with IVP

As a first example, consider the following first-order IVP:

$$y'(t) - f_1(t)y(t) = r(t), \quad y(t_1) = v_1, \quad t_1 \le t \le t_n.$$
 (39)

Then start by assuming the approximate solution to be of the form $\hat{y}(t) = \boldsymbol{\omega}^T \boldsymbol{\varphi}(t) + b$. In the NLS-SVMs framework, the approximate solution can be obtained by solving the following optimization problem:

minimize
$$\frac{1}{2}\boldsymbol{\omega}^{T}\boldsymbol{\omega} + \frac{\gamma}{2}\sum_{i=1}^{n}e_{i}^{2}$$
s.t.
$$y'(t_{i}) = \boldsymbol{\omega}^{T}\boldsymbol{\varphi}'(t_{i}) = f_{1}(t_{i})\left[\boldsymbol{\omega}^{T}\boldsymbol{\varphi}(t_{i}) + b\right] + r(t_{i}) + \boldsymbol{e}_{i}, \quad i = 2, \dots, n$$

$$y(t_{1}) = \boldsymbol{\omega}^{T}\boldsymbol{\varphi}(t_{1}) + b = v_{1}$$

$$(40)$$

The Lagrangian of the constrained optimization problem becomes

$$L(\omega, b, \lambda) = \frac{1}{2}\omega^{T}\omega + \frac{\gamma}{2}\left(\omega^{T}\varphi'(t_{i}) - f_{1}(t_{i})\left[\omega^{T}\varphi(t_{i}) + b\right] - r(t_{i})\right)^{T}$$

$$\cdot \left(\omega^{T}\varphi'(t_{i}) - f_{1}(t_{i})\left[\omega^{T}\varphi(t_{i}) + b\right] - r(t_{i})\right)$$

$$+ \lambda\left(\omega^{T}\varphi(t_{1}) + b - v_{1}\right)$$
(41)

Then the Karush–Kuhn–Tucker (KKT) optimality conditions are as follows: $\frac{\partial L(\omega,b,\lambda)}{\partial \omega} = 0$, $\frac{\partial L(\omega,b,\lambda)}{\partial b} = 0$, therefore, the solution to Eq.(41) is obtained by solving the following primary problem:

$$\begin{bmatrix} \mathbf{E} + \mathbf{A} (\mathbf{\Psi}' - \mathbf{f} \cdot \mathbf{\Psi}) & -\mathbf{A} (\mathbf{f} \cdot \mathbf{1}) & -\varphi^{T} (t_{1}) \\ \mathbf{V} (\mathbf{\Psi}' - \mathbf{f} \cdot \mathbf{\Psi}) & -\mathbf{V} (\mathbf{f} \cdot \mathbf{1}) & -1 \\ \varphi (t_{1}) & 1 & 0 \end{bmatrix} \begin{bmatrix} \boldsymbol{\omega} \\ \boldsymbol{b} \\ \boldsymbol{\lambda} \end{bmatrix} = \begin{bmatrix} \mathbf{A} \mathbf{r} \\ \mathbf{V} \mathbf{r} \\ v_{1} \end{bmatrix}$$
(42)

where $\boldsymbol{E} \in \mathbb{R}^{q \times q}$ is an identity matrix; $\boldsymbol{\Psi} = [\varphi(t_2),...,\varphi(t_n)]^T \in \mathbb{R}^{(n-1) \times m}; \ \boldsymbol{\Psi}' = [\varphi'(t_2),...,\varphi'(t_n)]^T \in \mathbb{R}^{(n-1) \times m}; \ \boldsymbol{f} = [f_1(t_2),...,f_1(t_n)]^T \in \mathbb{R}^{n-1}; \ \boldsymbol{1} = [1,...,1]^T \in \mathbb{R}^{n-1}; \ \boldsymbol{\varphi}(t_1) \in \mathbb{R}^{1 \times m}; \boldsymbol{A} = \gamma [\boldsymbol{\Psi}' - \boldsymbol{f} \boldsymbol{\Psi}]^T \in \mathbb{R}^{m \times (n-1)}; \boldsymbol{V} = \gamma [-\boldsymbol{f} \boldsymbol{1}]^T \in \mathbb{R}^{1 \times (n-1)}; \boldsymbol{r} = [r(t_2),...,r(t_n)]^T \in \mathbb{R}^{n-1}; \ \boldsymbol{\omega} \in \mathbb{R}^{m \times 1}; \ \boldsymbol{\gamma} \text{ is a regularization parameter.}$

The model in the primary form becomes $\hat{y}(t) = \boldsymbol{\omega}^T \boldsymbol{\varphi}(t) + b$

A.7 NLS-SVMs for Solving Second-Order ODEs with IVP and BVP

IVP Case Let us consider a second-order IVP of the form:

$$y''(t) = f_1(t)y'(t) + f_2(t)y(t) + r(t), \quad y(t_1) = v_1, \quad y'(t_1) = v_2, \quad t_1 \le t \le t_n.$$
 (43)

The approximate solution, $\hat{y}(t) = \omega^T \varphi(t) + b$, is then obtained by solving the following optimization problem:

minimize
$$\frac{1}{2}\boldsymbol{\omega}^{T}\boldsymbol{\omega} + \frac{\gamma}{2}\sum_{i=1}^{n}e_{i}^{2}$$
s.t.
$$y''(t_{i}) = \boldsymbol{\omega}^{T}\boldsymbol{\varphi}''(t_{i}) = f_{1}(t_{i})\boldsymbol{\omega}^{T}\boldsymbol{\varphi}'(t_{i}) + f_{2}(t_{i})\left[\boldsymbol{\omega}^{T}\boldsymbol{\varphi}(t_{i}) + b\right] + r(t_{i}) + \boldsymbol{e}_{i}$$

$$i = 2, \dots, n$$

$$y'(t_{1}) = \boldsymbol{\omega}^{T}\boldsymbol{\varphi}'(t_{1}) = v_{2}$$

$$y(t_{1}) = \boldsymbol{\omega}^{T}\boldsymbol{\varphi}(t_{1}) + b = v_{1}$$

$$(44)$$

The Lagrangian of the constrained optimization problem becomes

$$L(\boldsymbol{\omega}, b, \lambda_{1}, \lambda_{2}) = \frac{1}{2} \boldsymbol{\omega}^{T} \boldsymbol{\omega} + \frac{\gamma}{2} \left(\boldsymbol{\omega}^{T} \boldsymbol{\varphi}''(t_{i}) - f_{1}(t_{i}) \boldsymbol{\omega}^{T} \boldsymbol{\varphi}'(t_{i}) - f_{2}(t_{i}) \left[\boldsymbol{\omega}^{T} \boldsymbol{\varphi}(t_{i}) + b \right] - \boldsymbol{r}(t_{i}) \right)^{T}$$

$$\left(\boldsymbol{\omega}^{T} \boldsymbol{\varphi}''(t_{i}) - f_{1}(t_{i}) \boldsymbol{\omega}^{T} \boldsymbol{\varphi}'(t_{i}) - f_{2}(t_{i}) \left[\boldsymbol{\omega}^{T} \boldsymbol{\varphi}(t_{i}) + b \right] - \boldsymbol{r}(t_{i}) \right)$$

$$+ \lambda_{1} \left(\boldsymbol{\omega}^{T} \boldsymbol{\varphi}(t_{1}) + b - v_{1} \right) + \lambda_{2} \left(\boldsymbol{\omega}^{T} \boldsymbol{\varphi}'(t_{1}) - v_{2} \right)$$

$$(45)$$

Then the Karush–Kuhn–Tucker (KKT) optimality conditions are as follows: $\frac{\partial L(\omega,b,\lambda_1,\lambda_2)}{\partial \omega} = 0$, $\frac{\partial L(\omega,b,\lambda_1,\lambda_2)}{\partial b} = 0$, $\frac{\partial L(\omega,b,\lambda_1,\lambda_2)}{\partial \lambda_1} = 0$, $\frac{\partial L(\omega,b,\lambda_1,\lambda_2)}{\partial \lambda_2} = 0$, therefore, the solution to Eq.(45) is obtained by solving the following primary problem:

$$\begin{bmatrix} \boldsymbol{E} + \mathbf{A} \left(\boldsymbol{\Psi}'' - \boldsymbol{f_1} \boldsymbol{\Psi}' - \boldsymbol{f_2} \boldsymbol{\Psi} \right) & -\mathbf{A} \left(\boldsymbol{f_2} \cdot \mathbf{1} \right) & \boldsymbol{\varphi}^T \left(t_1 \right) & \left(\boldsymbol{\varphi}'(t_1) \right)^T \\ \boldsymbol{V} \left(\boldsymbol{\Psi}'' - \boldsymbol{f_1} \boldsymbol{\Psi}' - \boldsymbol{f_2} \boldsymbol{\Psi} \right) & -\boldsymbol{V} \left(\boldsymbol{f_2} \cdot \mathbf{1} \right) & 1 & 0 \\ \boldsymbol{\varphi} \left(t_1 \right) & 1 & 0 & 0 \\ \boldsymbol{\varphi}'(t_1) & 1 & 0 & 0 \end{bmatrix} \begin{bmatrix} \boldsymbol{\omega} \\ \boldsymbol{b} \\ \lambda_1 \\ \lambda_2 \end{bmatrix} = \begin{bmatrix} \mathbf{A} \boldsymbol{r} \\ \boldsymbol{V} \boldsymbol{r} \\ v_1 \\ v_2 \end{bmatrix}$$

$$(46)$$

where $\boldsymbol{E} \in \mathbb{R}^{m \times m}$ is an identity matrix; $\boldsymbol{\Psi} = [\varphi(t_2), ..., \varphi(t_n)]^T \in \mathbb{R}^{(n-1) \times m};$ $\boldsymbol{\Psi}' = [\varphi'(t_2), ..., \varphi'(t_n)]^T \in \mathbb{R}^{(n-1) \times m};$ $\boldsymbol{\Phi}' = [\varphi'(t_2), ..., \varphi'(t_n)]^T \in \mathbb{R}^{(n-1) \times m};$ $\boldsymbol{f}_1 = [f_1(t_2), ..., f_1(t_n)]^T \in \mathbb{R}^{n-1};$ $\boldsymbol{f}_2 = [f_2(t_2), ..., f_2(t_n)]^T \in \mathbb{R}^{n-1};$ $\boldsymbol{1} = [1, ..., 1]^T \in \mathbb{R}^{n-1};$ $\boldsymbol{\varphi}(t_1) \in \mathbb{R}^{1 \times q}; \boldsymbol{\varphi}'(t_1) \in \mathbb{R}^{1 \times m}; \boldsymbol{A} = \gamma [\boldsymbol{\Psi}'' - \boldsymbol{f}_1 \boldsymbol{\Psi}' - \boldsymbol{f}_2 \boldsymbol{\Psi}]^T \in \mathbb{R}^{m \times (n-1)}; \boldsymbol{V} = \gamma [-\boldsymbol{f}_2 \boldsymbol{1}]^T \in \mathbb{R}^{1 \times (n-1)}; \boldsymbol{r} = [r(t_2), ..., r(t_n)]^T \in \mathbb{R}^{n-1};$ $\boldsymbol{\omega} \in \mathbb{R}^{m \times 1};$ $\boldsymbol{\gamma}$ is a regularization parameter.

The model in the primary form becomes $\hat{y}(t) = \omega^T \varphi(t) + b$.

BVP Case Consider the second-order BVP of ODEs of the form

$$y''(t) = f_1(t)y'(t) + f_2(t)y(t) + r(t), \quad y(t_1) = q_1, \quad y(t_n) = q_n, \quad t_1 \le t \le t_n.$$
 (47)

Then the parameters of the closed-form approximation of the solution can be obtained by solving the following optimization problem:

$$\underset{\boldsymbol{\omega},b,e_{i}}{\text{minimize}} \quad \frac{1}{2}\boldsymbol{\omega}^{T}\boldsymbol{\omega} + \frac{\gamma}{2}\sum_{i=1}^{n}e_{i}^{2}$$
s.t.
$$y''(t_{i}) = \boldsymbol{\omega}^{T}\boldsymbol{\varphi}''(t_{i}) = f_{1}(t_{i})\boldsymbol{\omega}^{T}\boldsymbol{\varphi}'(t_{i}) + f_{2}(t_{i})\left[\boldsymbol{\omega}^{T}\boldsymbol{\varphi}(t_{i}) + b\right] + r(t_{i}) + \boldsymbol{e}_{i}$$

$$i = 2, \dots, n-1$$

$$y(t_{1}) = \boldsymbol{\omega}^{T}\boldsymbol{\varphi}(t_{1}) + b = q_{1}$$

$$y(t_{n}) = \boldsymbol{\omega}^{T}\boldsymbol{\varphi}(t_{n}) + b = q_{n}$$
(48)

The same procedure can be applied to derive the Lagrangian and afterward the KKT optimality conditions. Then, one can show that the solution to Eq.(48) is obtained by solving the following linear system:

$$\begin{bmatrix} \boldsymbol{E} + \mathbf{A} \left(\boldsymbol{\Psi}'' - \boldsymbol{f_1} \boldsymbol{\Psi}' - \boldsymbol{f_2} \boldsymbol{\Psi} \right) & -\mathbf{A} \left(\boldsymbol{f_2} \cdot \boldsymbol{1} \right) & \boldsymbol{\varphi}^T \left(t_1 \right) & \boldsymbol{\varphi}^T \left(t_n \right) \\ \boldsymbol{V} \left(\boldsymbol{\Psi}'' - \boldsymbol{f_1} \boldsymbol{\Psi}' - \boldsymbol{f_2} \boldsymbol{\Psi} \right) & -\boldsymbol{V} \left(\boldsymbol{f_2} \cdot \boldsymbol{1} \right) & 1 & 1 \\ \boldsymbol{\varphi} \left(t_1 \right) & 1 & 0 & 0 \\ \boldsymbol{\varphi} \left(t_n \right) & 1 & 0 & 0 \end{bmatrix} \begin{bmatrix} \boldsymbol{\omega} \\ \boldsymbol{b} \\ \lambda_1 \\ \lambda_2 \end{bmatrix} = \begin{bmatrix} \mathbf{A} \boldsymbol{r} \\ \boldsymbol{V} \boldsymbol{r} \\ q_1 \\ q_n \end{bmatrix}$$

$$(49)$$

where $\boldsymbol{E} \in \mathbb{R}^{m \times m}$ is an identity matrix; $\boldsymbol{\Psi} = [\varphi(t_2),...,\varphi(t_{n-1})]^T \in \mathbb{R}^{(n-2) \times m}; \boldsymbol{\Psi}' = [\varphi'(t_2),...,\varphi'(t_{n-1})]^T \in \mathbb{R}^{(n-2) \times m}; \boldsymbol{\Psi}'' = [\varphi''(t_2),...,\varphi''(t_{n-1})]^T \in \mathbb{R}^{(n-2) \times m}; \boldsymbol{f}_1 = [f_1(t_2),...,f_1(t_{n-1})]^T \in \mathbb{R}^{n-2}; \boldsymbol{f}_2 = [f_2(t_2),...,f_2(t_{n-1})]^T \in \mathbb{R}^{n-2}; \boldsymbol{1} = [1,...,1]^T \in \mathbb{R}^{n-2}; \boldsymbol{\varphi}(t_1) \in \mathbb{R}^{1 \times m}; \boldsymbol{\varphi}(t_n) \in \mathbb{R}^{1 \times m}; \boldsymbol{A} = \gamma [\boldsymbol{\Psi}'' - \boldsymbol{f}_1 \boldsymbol{\Psi}' - \boldsymbol{f}_2 \boldsymbol{\Psi}]^T \in \mathbb{R}^{m \times (n-2)}; \boldsymbol{V} = \gamma [-\boldsymbol{f}_2 \boldsymbol{1}]^T \in \mathbb{R}^{1 \times (n-2)}; \boldsymbol{r} = [r(t_2),...,r(t_n)]^T \in \mathbb{R}^{n-2}; \boldsymbol{\omega} \in \mathbb{R}^{m \times 1}; \gamma \text{ is a regularization parameter.}$

The model in the primary form becomes $\hat{y}(t) = \boldsymbol{\omega}^T \boldsymbol{\varphi}(t) + b$.

A.8 NLS-SVMs for Solving First-Order nonlinear ODE

Here, we take Eq.(3) as the object of study. The Lagrangian of the constrained optimization problem becomes

$$L(\boldsymbol{\omega}, b, \lambda, \boldsymbol{y}_i) = \frac{1}{2} \boldsymbol{\omega}^T \boldsymbol{\omega} + \frac{\gamma}{2} \left(\boldsymbol{\omega}^T \boldsymbol{\varphi}'(t_i) - f(t_i, y_i) \right)^T \left(\boldsymbol{\omega}^T \boldsymbol{\varphi}'(t_i) - f(t_i, y_i) \right) + \frac{\gamma}{2} \left(\boldsymbol{y}_i - \boldsymbol{\omega}^T \boldsymbol{\varphi}(t_i) - b \right)^T \left(\boldsymbol{y}_i - \boldsymbol{\omega}^T \boldsymbol{\varphi}(t_i) - b \right) + \lambda \left(\boldsymbol{\omega}^T \boldsymbol{\varphi}(t_1) + b - v_1 \right)$$
(50)

Then the Karush–Kuhn–Tucker (KKT) optimality conditions are as follows: $\frac{\partial L(\omega,b,\lambda,y_i)}{\partial \omega} = Y_1, \frac{\partial L(\omega,b,\lambda,y_i)}{\partial b} = Y_2, \frac{\partial L(\omega,b,\lambda,y_i)}{\partial \lambda} = Y_3, \frac{\partial L(\omega,b,\lambda,y_i)}{\partial y_i} = Y_4$, therefore, the solution to Eq.(50) is obtained by solving the following primary problem:

$$\begin{bmatrix} \frac{\partial \mathbf{Y}_{1}}{\partial \boldsymbol{\omega}} & \frac{\partial \mathbf{Y}_{1}}{\partial b} & \frac{\partial \mathbf{Y}_{1}}{\partial \lambda} & \frac{\partial \mathbf{Y}_{1}}{\partial \boldsymbol{y}_{i}} \\ \frac{\partial \mathbf{Y}_{2}}{\partial \boldsymbol{\omega}} & \frac{\partial \mathbf{Y}_{2}}{\partial b} & \frac{\partial \mathbf{Y}_{2}}{\partial \lambda} & \frac{\partial \mathbf{Y}_{2}}{\partial \boldsymbol{y}_{i}} \\ \frac{\partial \mathbf{Y}_{3}}{\partial \boldsymbol{\omega}} & \frac{\partial \mathbf{Y}_{3}}{\partial b} & \frac{\partial \mathbf{Y}_{3}}{\partial \lambda} & \frac{\partial \mathbf{Y}_{3}}{\partial \boldsymbol{y}_{i}} \\ \frac{\partial \mathbf{Y}_{4}}{\partial \boldsymbol{\omega}_{i}} & \frac{\partial \mathbf{Y}_{3}}{\partial b} & \frac{\partial \mathbf{Y}_{4}}{\partial \lambda} & \frac{\partial \mathbf{Y}_{4}}{\partial \boldsymbol{y}_{i}} \end{bmatrix} \begin{bmatrix} \boldsymbol{\omega} \\ \boldsymbol{b} \\ \boldsymbol{\lambda} \\ \boldsymbol{y}_{i} \end{bmatrix} = \begin{bmatrix} \boldsymbol{Y}_{1} \\ \boldsymbol{Y}_{2} \\ \boldsymbol{Y}_{3} \\ \boldsymbol{Y}_{4} \end{bmatrix}$$

$$(51)$$

where $Y1 \in \mathbb{R}^{m \times 1}$; $Y2 \in \mathbb{R}^{1 \times 1}$; $Y3 \in \mathbb{R}^{1 \times 1}$; $Y4 \in \mathbb{R}^{(n-1) \times 1}$. The nonlinear system, which consists of equations with unknowns $(\boldsymbol{\omega}, b, \lambda, \boldsymbol{y_i})$, is solved by Newton's method. The model in the primary form becomes $\hat{y}(t) = \boldsymbol{\omega}^T \boldsymbol{\varphi}(t) + b$.

B Supplementary Material

B.1 Sixteen benchmark ODE problems

Problem 1: Consider the first-order ODE with time varying coefficient [8, 36, 37] $y'(t) + \left(t + \frac{1+3t^2}{1+t+t^3}\right)y = t^3 + 2t + t^2\left(\frac{1+3t^2}{1+t+t^3}\right), t \in [0,3], y(0) = 1$

Problem 2: Consider the Dahlquist's problem as a non-stiff linear problem [38] given by $y'(t) = -y(t), t \in (0, 10], y(0) = 1$

Problem 3: Consider a well-known stiff test problem, the Prothero–Robinson equation [38, 39], $y'(t) = -10^3(y(t) - \sin t) + \cos t, t \in (0, 10]; y(0) = 0$

Problem 4: Consider the following nonlinear first-order ODE, which is studied by Junaid et al $[40], y'(t) = y(t) - \frac{t}{y(t)}, t \in (0,3], y(0) = 1$

Problem 5: Consider the following nonlinear first-order ODE [38] defined by $y'(t) = y^2(t), t \in (0,1], y(0) = -1$

Problem 6: Consider the following nonlinear first-order ODE [41] defined by $y'(t) = 2t^{-1}\sqrt{y(t) - \ln t} + t^{-1}, t \in (1, 1.2], y(1) = 0$

Problem 7: Consider the following second-order IVP [42] defined by y''(t) + 0.3y'(t) + y(t) = 1, $t \in (0, 20]$, y(0) = 0, y'(0) = 0, the interval solution for this test problem is considered from 0 to 20, which is assumed to be a wide range for solutions.

Problem 8: Consider the second ODE having the initial conditions based on the laws of physics as follows [42]: $\frac{1}{2}y''(t) + 18y(t) = 0, t \in (0, 2], y(0) = -\frac{1}{2}, y'(0) = 1$

Problem 9: Consider the following second order damped free vibration equation [36]: $y''(t) + 4y'(t) + 4y(t) = 0, t \in [0, 10], \quad y(0) = 1, y'(0) = 1$

Problem 10: Consider the following second-order ODE with time-varying input signal [37]: $y''(t) + \frac{1}{5}y'(t) + y(t) = -\frac{1}{5}e^{-(t/5)}\cos t, t \in [0, 10], y(0) = 0, y'(0) = 1$

Problem 11: Consider a second-order singular ordinary differential equation [43]: $y''(t) + \frac{1}{t}y'(t) + \cos(t) + \frac{\sin(t)}{t} = 0, t \in [0, 1], y(0) = 1, y(1) = \cos(1)$

Problem 12: Consider the following second-order ODE [44]: $y''(t) + y(t) = 2, t \in [0, 1], y(0) = 1, y(1) = 0$

Problem 13: Consider a singular differential equation [45, 43]: $y''(t) + \frac{1-2t}{t}y'(t) + \frac{t-1}{t}y(t) = 0, t \in [0, 1], y(0) = 1, y(1) = e$

Problem 14: Consider one of the most famous second order ODE. It is given as follows [42, 46]: $y''(t) + (y'(t))^2 - 2e^{-y(t)} = 0, t \in (0,1], y(0) = 0, y(1) = 0$

Problem 15: Consider the following nonlinear second-order ODE [41, 47] defined by $y''(t) = -y(t) + \frac{2(y'(t))^2}{y(t)}, t \in [-1, 1], y(-1) = y(1) = 0.324027137$

Problem 16: Consider a fourth-order linear ODE [48, 49] defined by $y^{(4)}(t) = 120t, t \in [-1, 1], y(-1) = 1, y'(-1) = 5, y(1) = 3, y'(1) = 5$

B.2 NLS-SVMs for Solving Second-order ODE in Terms of Problem 15

Problem15:
$$y''(t) = -y(t) + \frac{2(y'(t))^2}{y(t)}, t \in [-1, 1], y(-1) = y(1) = 0.324027137$$

$$\underset{\omega, b, e_i, \xi_i, y_i}{\text{minimize}} \frac{1}{2} \omega^T \omega + \frac{\gamma}{2} \sum_{i=1}^n e_i^2 + \frac{\gamma}{2} \sum_{i=1}^n \xi_i^2$$
(52)
$$\text{s.t. } y''(t_i) = \omega^T \varphi''(t_i) = -y(t_i) + 2(y'(t_i))^2 / y(t_i) + e_i, \quad i = 2, \dots, n-1$$

$$y'(t_i) = \omega^T \varphi'(t_i), \quad i = 2, \dots, n-1$$

$$y(t_i) = \omega^T \varphi(t_i) + b + \xi_i, \quad i = 2, \dots, n-1$$

$$\omega^T \varphi(t_i) + b = q_1$$

$$\omega^T \varphi(t_i) + b = q_n.$$

The Lagrangian of the constrained optimization problem becomes

$$L(\boldsymbol{\omega}, b, \lambda_1, \lambda_2, \boldsymbol{y}_i) = \frac{1}{2} \boldsymbol{\omega}^T \boldsymbol{\omega} + \frac{\gamma}{2} \left(\boldsymbol{w}^T \boldsymbol{\varphi}''(t_i) - (-y(t_i) + 2(y'(t_i))^2 / y(t_i)) \right)^T$$

$$\left(\boldsymbol{w}^T \boldsymbol{\varphi}''(t_i) - (-y(t_i) + 2(y'(t_i))^2 / y(t_i)) \right) + \frac{\gamma}{2} \left(\boldsymbol{y}_i - \boldsymbol{\omega}^T \boldsymbol{\varphi}(t_i) - b \right)^T$$

$$\left(\boldsymbol{y}_i - \boldsymbol{\omega}^T \boldsymbol{\varphi}(t_i) - b \right) + \lambda_1 \left(\boldsymbol{\omega}^T \boldsymbol{\varphi}(t_1) + b - q_1 \right) + \lambda_2 \left(\boldsymbol{\omega}^T \boldsymbol{\varphi}(t_N) + b - q_n \right)$$
(53)

Further simplified:

$$L(\boldsymbol{\omega}, b, \lambda_{1}, \lambda_{2}, \boldsymbol{y}_{i}) = \frac{1}{2} \boldsymbol{\omega}^{T} \boldsymbol{\omega} + \frac{\gamma}{2} \left(\boldsymbol{w}^{T} \boldsymbol{\varphi}''(t_{i}) - (-\boldsymbol{y}_{i} + 2(\boldsymbol{\omega}^{T} \boldsymbol{\varphi}'(t_{i}))^{2} / \boldsymbol{y}_{i} \right)^{T}$$

$$\left(\boldsymbol{w}^{T} \boldsymbol{\varphi}''(t_{i}) - (-\boldsymbol{y}_{i} + 2(\boldsymbol{\omega}^{T} \boldsymbol{\varphi}'(t_{i}))^{2} / \boldsymbol{y}_{i} \right) + \frac{\gamma}{2} \left(\boldsymbol{y}_{i} - \boldsymbol{\omega}^{T} \boldsymbol{\varphi}(t_{i}) - b \right)^{T}$$

$$\left(\boldsymbol{y}_{i} - \boldsymbol{\omega}^{T} \boldsymbol{\varphi}(t_{i}) - b \right) + \lambda_{1} \left(\boldsymbol{\omega}^{T} \boldsymbol{\varphi}(t_{1}) + b - q_{1} \right) + \lambda_{2} \left(\boldsymbol{\omega}^{T} \boldsymbol{\varphi}(t_{N}) + b - q_{n} \right)$$

$$(54)$$

Then the Karush–Kuhn–Tucker (KKT) optimality conditions are as follows:

$$Y1: \frac{\partial L(\boldsymbol{\omega}, b, \lambda_1, \lambda_2, \boldsymbol{y}_i)}{\partial \boldsymbol{\omega}} = \boldsymbol{\omega} + \gamma \left[(\boldsymbol{\varphi}_{t_i}^{"})^T [\boldsymbol{\varphi}_{t_i}^{"} \boldsymbol{\omega} - 2(\boldsymbol{\varphi}_{t_i}^{'} \boldsymbol{\omega})^2 / \boldsymbol{y}_i + \boldsymbol{y}_i] - 4(\boldsymbol{\varphi}_{t_i}^{'})^T [(\boldsymbol{\varphi}_{t_i}^{'} \boldsymbol{\omega} / \boldsymbol{y}_i) \odot (\boldsymbol{\varphi}_{t_i}^{"} \boldsymbol{\omega} - 2(\boldsymbol{\varphi}_{t_i}^{'} \boldsymbol{\omega})^2 / \boldsymbol{y}_i + \boldsymbol{y}_i)] \right] + \gamma [-\boldsymbol{\varphi}_{t_i}]^T [\boldsymbol{y}_i - \boldsymbol{\varphi}_{t_i} \boldsymbol{\omega} - b\boldsymbol{I}] + \lambda_1 \boldsymbol{\varphi}_{t_1} + \lambda_2 \boldsymbol{\varphi}_{t_n}$$
(55)

$$Y2: \frac{\partial L(\boldsymbol{\omega}, b, \lambda_1, \lambda_2, \boldsymbol{y}_i)}{\partial b} = \gamma [-\boldsymbol{I}]^T [\boldsymbol{y}_i - \boldsymbol{\varphi}_{t_i} \boldsymbol{\omega} - b\boldsymbol{I}] + \lambda_1 + \lambda_2$$
 (56)

$$\mathbf{Y}3: \frac{\partial L(\boldsymbol{\omega}, b, \lambda_1, \lambda_2, \boldsymbol{y}_i)}{\partial \lambda_1} = \boldsymbol{\varphi}_{t_1} \boldsymbol{\omega} + b - q_1$$
(57)

$$\mathbf{Y}4: \frac{\partial L(\boldsymbol{\omega}, b, \lambda_1, \lambda_2, \mathbf{y}_i)}{\partial \lambda_2} = \boldsymbol{\varphi}_{t_N} \boldsymbol{\omega} + b - q_n$$
(58)

$$Y5: \frac{\partial L(\boldsymbol{\omega}, b, \lambda_1, \lambda_2, \boldsymbol{y}_i)}{\partial \boldsymbol{y}_i} = \gamma \left[2(\boldsymbol{\varphi}'_{t_i} \boldsymbol{\omega})^2 / \boldsymbol{y}_i + 1 \right] \odot \left[\boldsymbol{\varphi}''_{t_i} \boldsymbol{\omega} - 2(\boldsymbol{\varphi}'_{t_i} \boldsymbol{\omega})^2 / \boldsymbol{y}_i + \boldsymbol{y}_i \right] + \gamma \left[\boldsymbol{y}_i - \boldsymbol{\varphi}_{t_i} \boldsymbol{\omega} - b \boldsymbol{I} \right]$$
(59)

Construct the Jacobian matrix and establish the matrix equation:

$$\begin{bmatrix} \frac{\partial Y_{1}}{\partial \boldsymbol{\omega}} & \frac{\partial Y_{1}}{\partial b} & \frac{\partial Y_{1}}{\partial \lambda_{1}} & \frac{\partial Y_{1}}{\partial \lambda_{2}} & \frac{\partial Y_{1}}{\partial y_{i}} \\ \frac{\partial Y_{2}}{\partial \boldsymbol{\omega}} & \frac{\partial Y_{3}}{\partial b} & \frac{\partial Y_{2}}{\partial \lambda_{1}} & \frac{\partial Y_{2}}{\partial \lambda_{2}} & \frac{\partial Y_{2}}{\partial y_{2}} \\ \frac{\partial Y_{3}}{\partial \boldsymbol{\omega}} & \frac{\partial Y_{3}}{\partial b} & \frac{\partial Y_{3}}{\partial \lambda_{1}} & \frac{\partial Y_{3}}{\partial \lambda_{2}} & \frac{\partial Y_{3}}{\partial y_{i}} \\ \frac{\partial Y_{4}}{\partial \boldsymbol{\omega}} & \frac{\partial Y_{4}}{\partial b} & \frac{\partial Y_{4}}{\partial \lambda_{1}} & \frac{\partial Y_{4}}{\partial \lambda_{2}} & \frac{\partial Y_{4}}{\partial y_{i}} \\ \frac{\partial Y_{5}}{\partial \boldsymbol{\omega}} & \frac{\partial Y_{5}}{\partial b} & \frac{\partial Y_{5}}{\partial \lambda_{1}} & \frac{\partial Y_{5}}{\partial \lambda_{2}} & \frac{\partial Y_{5}}{\partial y_{i}} \end{bmatrix} \begin{bmatrix} \boldsymbol{\omega} \\ b \\ \lambda_{1} \\ \lambda_{2} \\ y_{i} \end{bmatrix} = \begin{bmatrix} \boldsymbol{Y}_{1} \\ Y_{2} \\ Y_{3} \\ Y_{4} \\ Y_{5} \end{bmatrix}$$

$$(60)$$

Fill the results of the Jacobian matrix calculation into the equation matrix:

$$\begin{bmatrix} \frac{\partial \mathbf{Y}_{1}}{\partial \boldsymbol{\omega}} & \gamma(\boldsymbol{\varphi}'_{t_{i}})^{T} \mathbf{I} & (\boldsymbol{\varphi}'_{1})^{T} & (\boldsymbol{\varphi}'_{n})^{T} & \frac{\partial Y_{1}}{\partial \boldsymbol{y}_{i}} \\ \gamma \mathbf{I}^{T} \boldsymbol{\varphi}'_{t_{i}} & \gamma \mathbf{I}^{T} \mathbf{I} & 1 & 1 & \frac{\partial Y_{2}}{\partial \boldsymbol{y}_{i}} \\ \boldsymbol{\varphi}'_{1} & 1 & 0 & 0 & \frac{\partial Y_{3}}{\partial \boldsymbol{y}_{i}} \\ \boldsymbol{\varphi}'_{n} & 1 & 0 & 0 & \frac{\partial Y_{4}}{\partial \boldsymbol{y}_{i}} \\ \frac{\partial Y_{5}}{\partial \boldsymbol{w}} & -\gamma \mathbf{I} & \mathbf{0} & \mathbf{0} & \frac{\partial Y_{5}}{\partial \boldsymbol{y}_{i}} \end{bmatrix} \begin{bmatrix} \boldsymbol{\omega} \\ \boldsymbol{b} \\ \lambda_{1} \\ \lambda_{2} \\ \boldsymbol{y}_{i} \end{bmatrix} = \begin{bmatrix} \boldsymbol{Y}_{1} \\ Y_{2} \\ Y_{3} \\ Y_{4} \\ \boldsymbol{Y}_{5} \end{bmatrix}$$
(61)

where

$$\frac{\partial \mathbf{Y}1}{\partial \boldsymbol{\omega}} = \mathbf{E} + \gamma (\boldsymbol{\varphi}_{t_i}^{"})^T [\boldsymbol{\varphi}_{t_i}^{"} - 4\operatorname{diag}\left[\frac{\boldsymbol{\varphi}_{t_i}^{'}\boldsymbol{\omega}}{\boldsymbol{y}_i}\right] \boldsymbol{\varphi}_{t_i}^{'}\right] - 4\gamma (\boldsymbol{\varphi}_{t_i}^{'})^T \left[\operatorname{diag}\left[\frac{\boldsymbol{\varphi}_{t_i}^{'}\boldsymbol{\omega}}{\boldsymbol{y}_i}\right] \left[\boldsymbol{\varphi}_{t_i}^{"} - 4\operatorname{diag}\left[\frac{\boldsymbol{\varphi}_{t_i}^{'}\boldsymbol{\omega}}{\boldsymbol{y}_i}\right] \boldsymbol{\varphi}_{t_i}^{'}\right]\right] + \operatorname{diag}\left[\left[\boldsymbol{\varphi}_{t_i}^{"}\boldsymbol{\omega} - \frac{2(\boldsymbol{\varphi}_{t_i}^{'}\boldsymbol{\omega})^2}{\boldsymbol{y}_i} + \boldsymbol{y}_i\right]\operatorname{diag}\left[\frac{1}{\boldsymbol{y}_i}\right] \boldsymbol{\varphi}_{t_i}^{'}\right] + \gamma (\boldsymbol{\varphi}_{t_i})^T \boldsymbol{\varphi}_{t_i} \tag{62}$$

$$\frac{\partial \mathbf{Y}1}{\partial \mathbf{y}_{i}} = \gamma \boldsymbol{\varphi}_{t_{i}}^{"T} \operatorname{diag} \left[\frac{2(\boldsymbol{\varphi}_{t_{i}}^{'}\boldsymbol{\omega})^{2}}{\mathbf{y}_{i}^{2}} + 1 \right] \\
-4\gamma \boldsymbol{\varphi}_{t_{i}}^{"T} \operatorname{diag} \left[-\frac{\boldsymbol{\varphi}_{t_{i}}^{'}\boldsymbol{\omega} \odot \left[\boldsymbol{\varphi}_{t_{i}}^{"}\boldsymbol{\omega} - \frac{2(\boldsymbol{\varphi}_{t_{i}}^{'}\boldsymbol{\omega})^{2}}{\mathbf{y}_{i}} + \mathbf{y}_{i} \right]}{\mathbf{y}_{i}^{2}} + \frac{\boldsymbol{\varphi}_{t_{i}}^{'}\boldsymbol{\omega}}{\mathbf{y}_{i}} \odot \left[\frac{2(\boldsymbol{\varphi}_{t_{i}}^{'}\boldsymbol{\omega})^{2}}{\mathbf{y}_{i}} + 1 \right] \right] - \gamma \boldsymbol{\varphi}_{t_{i}}^{T} \tag{63}$$

$$\frac{\partial \mathbf{Y}5}{\partial \boldsymbol{\omega}} = \gamma \left[\operatorname{diag} \left[\frac{2(\boldsymbol{\varphi}'_{t_i} \boldsymbol{\omega})^2}{\boldsymbol{y}_i} + 1 \right] \left[\boldsymbol{\varphi}''_{t_i} - 4 \operatorname{diag} \left[\frac{\boldsymbol{\varphi}'_{t_i} \boldsymbol{\omega}}{\boldsymbol{y}_i} \right] \boldsymbol{\varphi}'_{t_i} \right] \right]
+ \gamma \left[\operatorname{diag} \left[\boldsymbol{\varphi}''_{t_i} \boldsymbol{\omega} - \frac{2(\boldsymbol{\varphi}'_{t_i} \boldsymbol{\omega})^2}{\boldsymbol{y}_i} + \boldsymbol{y}_i \right] 4 \operatorname{diag} \left[\frac{\boldsymbol{\varphi}'_{t_i} \boldsymbol{\omega}}{\boldsymbol{y}_i} \right] \boldsymbol{\varphi}'_{t_i} \right] - \gamma \boldsymbol{\varphi}_{t_i}$$
(64)

$$\frac{\partial \mathbf{Y}5}{\partial \mathbf{y}_{i}} = \gamma \operatorname{diag}\left[-\frac{2(\boldsymbol{\varphi}_{t_{i}}^{\prime}\boldsymbol{\omega})^{2}}{\mathbf{y}_{i}^{2}}\left[\boldsymbol{\varphi}_{t_{i}}^{\prime\prime}\boldsymbol{\omega} - \frac{2(\boldsymbol{\varphi}_{t_{i}}^{\prime}\boldsymbol{\omega})^{2}}{\mathbf{y}_{i}} + \mathbf{y}_{i}\right] + \left[\frac{2(\boldsymbol{\varphi}_{t_{i}}^{\prime}\boldsymbol{\omega})^{2}}{\mathbf{y}_{i}} + 1\right]\left[\frac{2(\boldsymbol{\varphi}_{t_{i}}^{\prime}\boldsymbol{\omega})^{2}}{\mathbf{y}_{i}^{2}} + 1\right] + 1\right]$$
(65)

Use Newton's iteration to solve for ω and b, and then construct the prediction equation in the original space: $\hat{y}(t) = \omega^T \varphi(t) + b$.

B.3 RBF kernel justification, Sampling for Nyström landmarks and PINN baseline comparison

Table 4: Comparative performance evaluation of Linear, Polynomial, and RBF Kernels for NLS-SVMs in Solving ODEs

| ODEs | Model | MAE | RMSE | $\ y - \hat{y}\ _{\infty}$ |
|-------------------------|--------|-----------------------|-----------------------|----------------------------|
| | Linear | 1.70×10 ⁰ | 2.00×10 ⁰ | 5.05×10 ⁰ |
| $Problem\ 1$ | Poly | 1.92×10 ⁻² | 2.45×10 ⁻² | 1.29×10^{-1} |
| | RBF | 7.94×10^{-4} | 9.47×10^{-4} | 1.87×10^{-3} |
| Problem 2 | Linear | 1.54×10^{0} | 2.15×10 ⁰ | 1.13×10 ¹ |
| Prootem 2 | Poly | 3.37×10^{-1} | 3.91×10^{-1} | 7.44×10^{-1} |
| | RBF | 3.16×10^{-6} | 3.77×10^{-6} | 9.75×10 ⁻⁶ |
| $\overline{Problem\ 3}$ | Linear | 6.34×10 ⁻¹ | 7.15×10 ⁻¹ | 1.24×10^{0} |
| 1 rootent 5 | Poly | 1.19×10 ⁻¹ | 1.43×10 ⁻¹ | 4.80×10^{-1} |
| | RBF | 2.06×10^{-8} | 2.77×10^{-8} | 1.40×10^{-7} |
| ${Problem 4}$ | Linear | 3.29×10^{0} | 4.67×10^{0} | 1.24×10 ¹ |
| Frontem 4 | Poly | 3.16×10^{0} | 4.45×10^{0} | 1.16×10^{1} |
| | RBF | 5.47×10^{-4} | 6.92×10^{-4} | 1.50×10^{-3} |
| Problem 5 | Linear | 1.07×10^{0} | 1.44×10^{0} | 5.82×10^{0} |
| 1 rootent 5 | Poly | 1.53×10^{-3} | 1.76×10^{-3} | 2.84×10^{-3} |
| | RBF | 8.79×10^{-4} | 1.07×10^{-3} | 1.67×10^{-3} |
| Problem 6 | Linear | 4.01×10^{0} | 5.05×10^{0} | 1.67×10 ¹ |
| r rootem o | Poly | 9.67×10 ⁻⁴ | 1.10×10^{-3} | 1.85×10^{-3} |
| | RBF | 8.89×10^{-4} | 1.01×10^{-3} | 1.70×10^{-3} |
| ${Problem 7}$ | Linear | 4.68×10 ⁻¹ | 6.05×10 ⁻¹ | 1.56×10 ⁰ |
| 1 rootent i | Poly | 3.82×10 ⁻¹ | 5.52×10 ⁻¹ | 1.47×10^{0} |
| | RBF | 1.43×10^{-3} | 1.67×10^{-3} | 3.02×10^{-3} |
| ${Problem8}$ | Linear | 4.30×10 ⁻¹ | 5.23×10 ⁻¹ | 2.01×10^{0} |
| 1 rootent 8 | Poly | 3.42×10^{-1} | 3.93×10 ⁻¹ | 6.70×10^{-1} |
| | RBF | 5.66×10^{-5} | 7.05×10^{-5} | 2.23×10^{-4} |
| $\overline{Problem 9}$ | Linear | 1.91×10^{0} | 2.60×10^{0} | 1.59×10 ¹ |
| 1 rootent s | Poly | 8.05×10^{-1} | 9.67×10 ⁻¹ | 1.73×10^{0} |
| | RBF | 5.74×10^{-5} | 6.92×10^{-5} | 2.21×10^{-4} |
| Problem 10 | Linear | 1.17×10 ⁰ | 1.61×10 ⁰ | 8.50×10 ⁰ |
| 1 / 00/0/// 10 | Poly | 5.23×10 ⁻¹ | 6.25×10^{-1} | 1.36×10^{0} |
| | RBF | 4.29×10^{-8} | 6.06×10^{-8} | 3.09×10^{-8} |
| Problem 11 | Linear | 9.62×10 ⁻² | 1.27×10 ⁻¹ | 5.79×10 ⁻¹ |
| 1 1000011111 | Poly | 7.13×10 ⁻⁴ | 8.90×10 ⁻⁴ | 1.60×10^{-3} |
| | RBF | 2.36×10 ⁻⁹ | 2.97×10 ⁻⁹ | 9.43×10 ⁻⁹ |
| | | | | |

| ODEs | Model | MAE | RMSE | $\ y - \hat{y}\ _{\infty}$ |
|------------------------|-----------------------|--|--|---|
| $\overline{Problem12}$ | Linear | 9.75×10 ⁻¹ | 1.27×10 ⁰ | 5.54×10 ⁰ |
| | Poly | 2.75×10 ⁻³ | 3.24×10 ⁻³ | 5.02×10 ⁻³ |
| | RBF | 3.15×10 ⁻⁹ | 3.94×10 ⁻⁹ | 1.31×10 ⁻⁸ |
| Problem 13 | Linear | 4.55×10 ⁰ | 6.58×10 ⁰ | 2.84×10 ¹ |
| | Poly | 1.27×10 ⁻³ | 1.59×10 ⁻³ | 2.91×10 ⁻³ |
| | RBF | 3.48×10 ⁻³ | 4.36×10 ⁻³ | 1.45×10 ⁻⁶ |
| Problem 14 | Linear Poly RBF | 2.12×10 ² 2.38×10 ⁻² 1.17×10 ⁻⁶ | 2.63×10 ² 2.82×10 ⁻² 1.57×10 ⁻⁶ | 7.68×10^{2} 4.42×10^{-2} 3.85×10^{-6} |
| Problem 15 | Linear | 1.08×10 ⁻¹ | 1.22×10 ⁻¹ | 1.76×10 ⁻¹ |
| | Poly | 2.93×10 ⁻¹ | 3.30×10 ⁻¹ | 7.96×10 ⁻¹ |
| | RBF | 1.68×10 ⁻⁷ | 1.98×10 ⁻⁷ | 3.46×10 ⁻⁷ |
| Problem 16 | Linear Poly RBF | 4.27×10^{15} 1.67×10^{-1} 1.72×10^{-5} | 6.18×10^{15} 1.92×10^{-1} 2.06×10^{-5} | 3.53×10 ¹⁶ 2.86×10 ⁻¹ 5.07×10 ⁻⁵ |

Table 5: Comparative performance evaluation of NLS-SVMs utilizing Equidistant, Random, and Leverage-based sampling strategies for solving ODEs

| ODEs | Model | MAE | RMSE | $\ y - \hat{y}\ _{\infty}$ | Time/s |
|-------------------------|---|---|---|---|----------------------|
| Problem 1 | Random | 8.70×10 ⁻⁴ | 1.06×10 ⁻³ | 3.06×10 ⁻³ | 0.52 |
| | Leverage score | 7.94×10 ⁻⁴ | 9.47×10 ⁻⁴ | 1.87×10 ⁻³ | 0.64 |
| | Equidistant | 7.94×10 ⁻⁴ | 9.47×10 ⁻⁴ | 1.87×10 ⁻³ | 0.55 |
| $\overline{Problem\ 2}$ | Random | 3.41×10 ⁻⁶ | 4.06×10 ⁻⁶ | 8.14×10 ⁻⁶ | 0.52 |
| | Leverage score | 3.22×10 ⁻⁶ | 3.82×10 ⁻⁶ | 7.51×10 ⁻⁶ | 0.57 |
| | Equidistant | 3.16×10 ⁻⁶ | 3.77×10 ⁻⁶ | 9.75×10 ⁻⁶ | 0.55 |
| $\overline{Problem\ 3}$ | Random | 1.31×10 ⁻⁷ | 1.75×10 ⁻⁷ | 8.99×10 ⁻⁷ | 0.53 |
| | Leverage score | 3.12×10 ⁻⁸ | 4.02×10 ⁻⁸ | 1.79×10 ⁻⁷ | 0.53 |
| | Equidistant | 2.06×10 ⁻⁸ | 2.77×10 ⁻⁸ | 1.40×10 ⁻⁷ | 0.56 |
| $\overline{Problem4}$ | Random Leverage score Equidistant | 5.47×10 ⁻⁴ 5.47×10 ⁻⁴ 5.47×10 ⁻⁴ | 6.92×10 ⁻⁴ 6.92×10 ⁻⁴ 6.92×10 ⁻⁴ | 1.50×10^{-3} 1.50×10^{-3} 1.50×10^{-3} | 9.53 14.1 10.2 |
| Problem 5 | Random | 8.79×10 ⁻⁴ | 1.07×10 ⁻³ | 1.67×10 ⁻³ | 1.07 |
| | Leverage score | 8.79×10 ⁻⁴ | 1.07×10 ⁻³ | 1.67×10 ⁻³ | 1.02 |
| | Equidistant | 8.79×10 ⁻⁴ | 1.07×10 ⁻³ | 1.67×10 ⁻³ | 0.97 |
| Problem 6 | Random | 8.89×10 ⁻⁴ | 1.01×10 ⁻³ | 1.70×10 ⁻³ | 0.80 |
| | Leverage score | 8.88×10 ⁻⁴ | 1.01×10 ⁻³ | 1.70×10 ⁻³ | 1.45 |
| | Equidistant | 8.89×10 ⁻⁴ | 1.01×10 ⁻³ | 1.70×10 ⁻³ | 0.69 |
| $\overline{Problem7}$ | Random | 1.43×10 ⁻³ | 1.66×10 ⁻³ | 3.02×10 ⁻³ | 0.45 |
| | Leverage score | 1.43×10 ⁻³ | 1.66×10 ⁻³ | 3.02×10 ⁻³ | 0.54 |
| | Equidistant | 1.43×10 ⁻³ | 1.67×10 ⁻³ | 3.02×10 ⁻³ | 0.50 |
| Problem 8 | Random | 9.92×10 ⁻⁵ | 1.29×10 ⁻⁴ | 4.87×10 ⁻⁴ | 0.44 |
| | Leverage score | 6.90×10 ⁻⁵ | 8.79×10 ⁻⁵ | 3.02×10 ⁻⁴ | 0.46 |
| | Equidistant | 5.66×10 ⁻⁵ | 7.05×10 ⁻⁵ | 2.23×10 ⁻⁴ | 0.44 |
| $\overline{Problem9}$ | Random | 8.43×10 ⁻⁵ | 1.15×10 ⁻⁴ | 3.88×10 ⁻⁴ | 0.43 |
| | Leverage score | 6.07×10 ⁻⁵ | 7.54×10 ⁻⁵ | 2.45×10 ⁻⁴ | 0.45 |
| | Equidistant | 5.74×10 ⁻⁵ | 6.92×10 ⁻⁵ | 2.21×10 ⁻⁴ | 0.47 |
| Problem 10 | Random | 1.63×10 ⁻⁷ | 2.25×10 ⁻⁷ | 1.05×10 ⁻⁶ | 0.44 |
| | Leverage score | 2.29×10 ⁻⁷ | 2.65×10 ⁻⁷ | 8.12×10 ⁻⁷ | 0.43 |
| | Equidistant | 4.29×10 ⁻⁸ | 6.06×10 ⁻⁸ | 3.09×10 ⁻⁸ | 0.49 |
| Problem 11 | Random | 9.02×10 ⁻⁹ | 1.08×10 ⁻⁸ | 2.90×10 ⁻⁸ | 0.43 |
| | Leverage score | 2.46×10 ⁻⁹ | 3.06×10 ⁻⁹ | 8.66×10 ⁻⁹ | 0.42 |

| ODEs | Model | MAE | RMSE | $\ y - \hat{y}\ _{\infty}$ | Time/s |
|-------------|----------------|-----------------------|-----------------------|----------------------------|--------|
| | Equidistant | 2.36×10 ⁻⁹ | 2.97×10 ⁻⁹ | 9.43×10 ⁻⁹ | 0.45 |
| Problem 12 | Random | 2.87×10 ⁻⁸ | 3.59×10 ⁻⁸ | 1.13×10 ⁻⁷ | 0.42 |
| 1 rootem 12 | Leverage score | 1.35×10^{-7} | 1.68×10^{-7} | 6.31×10^{-7} | 0.42 |
| | Equidistant | 3.15×10^{-9} | 3.94×10^{-9} | 1.31×10^{-8} | 0.46 |
| Problem 13 | Random | 8.76×10 ⁻⁷ | 1.13×10 ⁻⁶ | 4.29×10 ⁻⁶ | 0.42 |
| Frontem 13 | Leverage score | 5.48×10^{-7} | 6.89×10^{-7} | 2.28×10^{-6} | 0.42 |
| | Equidistant | 3.48×10^{-7} | 4.36×10^{-7} | 1.45×10^{-6} | 0.48 |
| Problem 14 | Random | 2.07×10 ⁻⁶ | 2.67×10 ⁻⁶ | 7.13×10 ⁻⁶ | 1.38 |
| 1 rootem 14 | Leverage score | 1.95×10^{-6} | 2.63×10^{-6} | 6.66×10^{-6} | 1.39 |
| | Equidistant | 1.17×10^{-6} | 1.57×10^{-6} | 3.85×10^{-6} | 1.39 |
| Problem 15 | Random | 1.99×10 ⁻⁷ | 2.35×10 ⁻⁷ | 4.40×10 ⁻⁷ | 3.54 |
| Frontem 15 | Leverage score | 1.73×10 ⁻⁷ | 2.04×10^{-7} | 3.60×10^{-7} | 3.19 |
| | Equidistant | 1.68×10^{-7} | 1.98×10^{-7} | 3.46×10^{-7} | 3.25 |
| Problem 16 | Random | 3.57×10 ⁻⁴ | 4.42×10 ⁻⁴ | 1.54×10 ⁻³ | 0.43 |
| r rootem 10 | Leverage score | 2.09×10^{-5} | 2.57×10^{-5} | 8.33×10^{-5} | 0.45 |
| | Equidistant | 1.72×10 ⁻⁵ | 2.06×10 ⁻⁵ | 5.07×10 ⁻⁵ | 0.42 |
| | | | | | |

 $\label{thm:comparative} \mbox{Table 6: Comparative performance evaluation of NLS-SVMs, RK4, and EAB methods for solving ODEs$

| ODEs | Model | MAE | RMSE | Train/s | Predict/s |
|-------------------------|----------|-----------------------|-----------------------|---------|-----------|
| Problem 1 | NLS-SVMs | 7.94×10 ⁻⁴ | 9.47×10 ⁻⁴ | 0.550 | 0.001 |
| Prootem 1 | RK4 | 2.20×10^{-5} | 1.80×10^{-5} | 0.011 | 0.011 |
| | EAB | 3.23×10 ⁻⁴ | 1.74×10^{-4} | 0.013 | 0.013 |
| $\overline{Problem\ 2}$ | NLS-SVMs | 3.16×10 ⁻⁶ | 3.77×10 ⁻⁶ | 0.480 | 0.002 |
| 1 rootent 2 | RK4 | 1.42×10^{-7} | 8.96×10 ⁻⁸ | 0.019 | 0.019 |
| | EAB | 2.93×10^{-3} | 1.36×10^{-3} | 0.021 | 0.021 |
| $\overline{Problem\ 3}$ | NLS-SVMs | 2.06×10 ⁻⁸ | 2.77×10 ⁻⁸ | 0.460 | 0.001 |
| 1 rootem 3 | RK4 | 3.87×10^{-7} | 3.41×10^{-7} | 0.880 | 0.880 |
| | EAB | 4.97×10^{-8} | 2.90×10^{-8} | 0.030 | 0.030 |
| $\overline{Problem 4}$ | NLS-SVMs | 5.47×10 ⁻⁴ | 6.92×10 ⁻⁴ | 14.530 | 0.001 |
| 1 rootem 4 | RK4 | 3.79×10^{-6} | 2.78×10^{-6} | 0.022 | 0.022 |
| | EAB | 9.41×10^{-4} | 6.45×10^{-4} | 0.016 | 0.016 |
| Problem 5 | NLS-SVMs | 8.79×10 ⁻⁴ | 1.07×10 ⁻³ | 4.590 | 0.001 |
| Problem~5 | RK4 | 3.58×10^{-7} | 3.38×10^{-7} | 0.013 | 0.013 |
| | EAB | 1.79×10 ⁻⁴ | 1.41×10^{-4} | 0.011 | 0.011 |
| Problem 6 | NLS-SVMs | 8.89×10 ⁻⁴ | 1.01×10 ⁻³ | 1.230 | 0.001 |
| 1 rootent o | RK4 | 7.94×10^{-2} | 5.61×10^{-2} | 0.021 | 0.021 |
| | EAB | 1.28×10^{-6} | 1.11×10^{-6} | 0.036 | 0.036 |
| Problem 7 | NLS-SVMs | 1.43×10 ⁻³ | 1.67×10 ⁻³ | 0.150 | 0.001 |
| 1 rootent i | RK4 | 1.66×10^{-3} | 1.42×10^{-3} | 0.012 | 0.012 |
| | EAB | 4.01×10^{-3} | 3.49×10^{-3} | 0.013 | 0.013 |
| Problem 8 | NLS-SVMs | 5.66×10 ⁻⁵ | 7.05×10 ⁻⁵ | 0.066 | 0.001 |
| rrootem 8 | RK4 | 3.61×10^{-3} | 2.81×10^{-3} | 0.023 | 0.023 |
| | EAB | 1.26×10^{-1} | 7.32×10^{-2} | 0.018 | 0.018 |
| $\overline{Problem 9}$ | NLS-SVMs | 5.74×10 ⁻⁵ | 6.92×10 ⁻⁵ | 0.170 | 0.001 |
| 1 Toolem 5 | RK4 | 8.21×10^{-6} | 3.08×10^{-6} | 0.022 | 0.022 |
| | EAB | 2.32×10^{-5} | 1.11×10^{-5} | 0.026 | 0.026 |
| $\overline{Problem10}$ | NLS-SVMs | 4.29×10 ⁻⁸ | 6.06×10 ⁻⁸ | 0.075 | 0.001 |
| 1 / 00/6/1/1/10 | RK4 | 1.00×10^{-6} | 1.00×10^{-6} | 0.029 | 0.029 |
| | EAB | 5.48×10 ⁻⁵ | 4.62×10 ⁻⁵ | 0.018 | 0.018 |

| Problem 11 | Model NLS-SVMs RK4 EAB | MAE 2.36×10 ⁻⁹ 3.11×10 ⁻⁶ 1.19×10 ⁻² | 2.97×10 ⁻⁹ 2.87×10 ⁻⁶ | Train/s 0.100 0.010 | 0.001 |
|----------------|---------------------------------|--|--|---------------------|-------|
| Problem 11 | RK4 EAB | 3.11×10 ⁻⁶ | 2.87×10 ⁻⁶ | | |
| | EAB | | | 0.010 | 0.010 |
| | | 1.19×10^{-2} | | 0.010 | 0.010 |
| | | | 6.86×10^{-3} | 0.020 | 0.020 |
| Problem 12 | NLS-SVMs | 3.15×10 ⁻⁹ | 3.94×10 ⁻⁹ | 0.043 | 0.001 |
| 1 / 0010/11 12 | RK4 | 5.75×10^{-7} | 5.20×10^{-7} | 0.016 | 0.016 |
| | EAB | 5.38×10^{-6} | 4.61×10^{-6} | 0.023 | 0.023 |
| Problem 13 | NLS-SVMs | 3.48×10 ⁻⁷ | 4.36×10 ⁻⁷ | 0.098 | 0.001 |
| 1 rootem 13 | RK4 | 1.57×10^{-6} | 1.21×10^{-6} | 0.011 | 0.011 |
| | EAB | 4.79×10^{-7} | 4.15×10^{-7} | 0.024 | 0.024 |
| Problem 14 | NLS-SVMs | 1.17×10 ⁻⁶ | 1.57×10 ⁻⁶ | 1.390 | 0.001 |
| 1 / 0016/11 14 | RK4 | 9.42×10^{-5} | 8.18×10^{-5} | 0.025 | 0.025 |
| | EAB | 9.75×10^{-4} | 7.57×10^{-4} | 0.019 | 0.019 |
| Problem 15 | NLS-SVMs | 1.68×10 ⁻⁷ | 1.98×10 ⁻⁷ | 1.690 | 0.001 |
| 1 rootem 15 | RK4 | 1.04×10^{-4} | 9.10×10^{-5} | 0.023 | 0.023 |
| | EAB | 1.35×10^{-4} | 9.89×10^{-5} | 0.020 | 0.020 |
| Problem 16 | NLS-SVMs | 1.72×10 ⁻⁵ | 2.06×10 ⁻⁵ | 0.410 | 0.001 |
| 1 1001611110 | RK4 | 3.75×10^{-4} | 4.89×10^{-4} | 0.019 | 0.019 |
| | EAB | 3.57×10^{-3} | 4.36×10 ⁻³ | 0.023 | 0.023 |

Table 7: Comparative performance evaluation of Vanilla PINN versus Fourier Feature-enhanced PINN for solving ODEs

| ODEs | Model | MAE | RMSE | $\ y - \hat{y}\ _{\infty}$ | Time/s |
|-------------------------|----------------------|-----------------------|-----------------------|----------------------------|---------|
| <u> </u> | | | 5.05×10 ⁻³ | 9.91×10^{-3} | |
| $Problem\ 1$ | Vanilla PINN | 4.45×10^{-3} | | | 672.00 |
| | Fourier Feature PINN | 1.02×10 ⁻² | 1.55×10 ⁻² | 3.41×10 ⁻² | 549.00 |
| $Problem\ 2$ | Vanilla PINN | 2.03×10 ⁻³ | 2.09×10 ⁻³ | 3.26×10^{-3} | 403.00 |
| | Fourier Feature PINN | 1.33×10 ⁻⁵ | 1.64×10^{-5} | 6.43×10^{-5} | 762.00 |
| Problem 3 | Vanilla PINN | 1.82×10 ⁻¹ | 2.88×10 ⁻¹ | 1.03×10^{0} | 1209.00 |
| 1 rootent 3 | Fourier Feature PINN | 8.51×10^{-4} | 1.15×10^{-3} | 3.72×10^{-3} | 1556.00 |
| ${Problem4}$ | Vanilla PINN | 5.35×10 ⁻¹ | 7.21×10 ⁻¹ | 1.81×10^{0} | 496.00 |
| 1 rootem 4 | Fourier Feature PINN | 5.57×10^{0} | 6.67×10^{0} | 1.50×10^{1} | 956.00 |
| $\overline{Problem\ 5}$ | Vanilla PINN | 1.03×10 ⁻³ | 1.04×10 ⁻³ | 1.13×10 ⁻³ | 166.00 |
| 1 rootem 5 | Fourier Feature PINN | 1.90×10^{-3} | 2.26×10^{-3} | 4.41×10^{-3} | 166.00 |
| Problem 6 | Vanilla PINN | 1.47×10 ⁻² | 1.76×10 ⁻² | 3.57×10 ⁻² | 75.60 |
| Problem 6 | Fourier Feature PINN | 2.32×10 ⁻² | 2.47×10^{-2} | 3.86×10^{1} | 217.00 |
| $\overline{Problem 7}$ | Vanilla PINN | 6.58×10 ⁻² | 8.06×10 ⁻² | 1.63×10 ⁻¹ | 1021.00 |
| Frontem 1 | Fourier Feature PINN | 7.88×10^{-1} | 8.35×10^{-1} | 1.42×10^{0} | 1279.00 |
| Problem 8 | Vanilla PINN | 5.23×10 ⁻³ | 5.92×10 ⁻³ | 1.04×10 ⁻² | 1392.00 |
| 1 rootem 6 | Fourier Feature PINN | 1.13×10^{-1} | 1.26×10^{-1} | 1.87×10^{-1} | 2170.00 |
| Problem 9 | Vanilla PINN | 8.66×10 ⁻⁵ | 9.96×10 ⁻⁵ | 1.89×10 ⁻⁴ | 776.00 |
| 1 rootem s | Fourier Feature PINN | 8.35×10^{-1} | 8.72×10^{-1} | 9.55×10^{-1} | 1534.00 |
| Problem 10 | Vanilla PINN | 3.12×10 ⁻² | 4.07×10 ⁻² | 8.62×10 ⁻² | 636.00 |
| Frontem 10 | Fourier Feature PINN | 2.61×10^{-1} | 3.31×10^{-1} | 7.02×10^{-1} | 2364.00 |
| Problem 11 | Vanilla PINN | 1.62×10 ⁻⁵ | 1.89×10 ⁻⁵ | 3.32×10 ⁻⁵ | 817.00 |
| Frontem 11 | Fourier Feature PINN | 2.81×10^{-8} | 3.48×10^{-8} | 1.16×10^{-7} | 16.30 |
| $\overline{Problem12}$ | Vanilla PINN | 2.28×10 ⁻⁵ | 2.29×10 ⁻⁵ | 2.60×10 ⁻⁵ | 969.00 |
| Frontem 12 | Fourier Feature PINN | 1.56×10^{-8} | 1.93×10 ⁻⁸ | 5.91×10^{-8} | 16.70 |
| Dnoblem 19 | Vanilla PINN | 4.22×10 ⁻³ | 5.72×10 ⁻³ | 1.05×10 ⁻² | 1475.00 |
| Problem~13 | Fourier Feature PINN | 2.77×10^{-7} | 3.42×10^{-7} | 9.56×10 ⁻⁷ | 33.60 |
| Problem 14 | Vanilla PINN | 8.22×10 ⁻⁶ | 8.77×10 ⁻⁶ | 1.34×10 ⁻⁵ | 112.40 |
| | | | Continued | on novt nogo | |

| ODEs | Model | MAE | RMSE | $\ y - \hat{y}\ _{\infty}$ | Time/s |
|------------|----------------------|-----------------------|-----------------------|----------------------------|---------|
| | Fourier Feature PINN | 7.38×10 ⁻⁷ | 9.17×10 ⁻⁷ | 2.02×10 ⁻⁶ | 36.00 |
| Problem 15 | Vanilla PINN | 2.42×10 ⁻³ | 2.62×10 ⁻³ | 3.62×10 ⁻³ | 230.00 |
| | Fourier Feature PINN | 2.14×10 ⁻⁸ | 2.66×10 ⁻⁸ | 6.68×10 ⁻⁷ | 85.40 |
| Problem 16 | Vanilla PINN | 1.24×10 ⁻² | 1.35×10 ⁻² | 1.80×10 ⁻² | 2699.00 |
| | Fourier Feature PINN | 7.51×10 ⁰ | 8.74×10 ⁰ | 2.38×10 ¹ | 697.00 |

B.4 Convergence analysis of iterative solver

Table 8: Convergence behavior and computational efficiency of NLS-SVMs across varying iteration counts for solving ODEs

| ODEs | Index | 50 | 100 | 200 | 300 | 400 | 500 |
|------------|-----------|-----------------------|-----------------------|-----------------------|-----------------------|-----------------------|-----------------------|
| Problem 4 | Residuals | 5.1×10 ⁻⁵ | 3.9×10 ⁻⁵ | 3.5×10 ⁻⁵ | 1.6×10 ⁻⁵ | 6.4×10 ⁻⁵ | 1.1×10 ⁻⁴ |
| | RMSE | 6.92×10 ⁻⁴ |
| | Time/s | 10.2 | 24.1 | 53.0 | 81.2 | 107.4 | 135.0 |
| Problem 5 | Residuals | 5.1×10 ¹ |
| | RMSE | 1.07×10 ⁻³ |
| | Time/s | 1.8 | 12.0 | 30.5 | 48.8 | 65.5 | 84.0 |
| Problem 6 | Residuals | 6.0×10 ⁻² |
| | RMSE | 1.01×10 ⁻³ |
| | Time/s | 0.7 | 0.9 | 1.7 | 2.9 | 5.4 | 7.7 |
| Problem 14 | Residuals | 5.1×10 ⁶ | 5.6×10 ⁵ | 6.4×10 ³ | 7.3×10 ¹ | 8.3×10 ⁻¹ | 9.5×10 ⁻³ |
| | RMSE | 4.97×10 ⁻⁴ | 5.36×10 ⁻⁵ | 1.84×10 ⁻⁶ | 1.58×10 ⁻⁶ | 1.57×10 ⁻⁶ | 1.57×10 ⁻⁶ |
| | Time/s | 0.6 | 0.7 | 0.8 | 1.0 | 1.3 | 1.4 |
| Problem 15 | Residuals | 1.9×10 ⁻³ | 1.4×10 ⁻⁶ | 8.6×10 ⁻⁶ | 2.9×10 ⁻⁶ | 2.5×10 ⁻⁶ | 7.1×10 ⁻⁶ |
| | RMSE | 1.98×10 ⁻⁷ |
| | Time/s | 0.8 | 0.9 | 1.3 | 2.2 | 3.3 | 6.6 |

B.5 Hyperparameters for Training

Table 9: Hyperparameter configurations for PINN, LS-SVMs and NLS-SVMs in solving ODEs

| ODEs | Model | Total sample | Sub-sample | Epoch/Iteration | σ^2 | γ |
|-------------------------|----------|--------------|------------|-----------------|------------|----------|
| Problem 1 | PINN | 1000 | - | 10000 | - | - |
| Prootem 1 | LS-SVMs | 1000 | - | - | 10 | 10^{7} |
| | NLS-SVMs | 100 | 150 | - | 10 | 10^{7} |
| Problem 2 | PINN | 10000 | - | 10000 | - | - |
| Frontem 2 | LS-SVMs | 10000 | - | - | 10 | 10^{7} |
| | NLS-SVMs | 10000 | 50 | - | 10 | 10^{7} |
| $\overline{Problem\ 3}$ | PINN | 10000 | - | 20000 | - | - |
| | LS-SVMs | 10000 | - | - | 10 | 10^{7} |
| | NLS-SVMs | 10000 | 50 | - | 10 | 10^{7} |
| Problem 4 | PINN | 1000 | - | 10000 | - | - |
| 1 rootem 4 | LS-SVMs | 1000 | - | 50 | 10 | 10^{6} |
| | NLS-SVMs | 1000 | 50 | 50 | 10 | 10^{6} |
| Problem 5 | PINN | 600 | - | 10000 | - | - |
| Problem 5 | LS-SVMs | 600 | - | 25 | 8 | 10^{6} |
| | NLS-SVMs | 600 | 20 | 25 | 8 | 10^{6} |
| Problem 6 | PINN | 300 | - | 10000 | - | - |
| r romem o | LS-SVMs | 300 | - | 50 | 1 | 10^{6} |

| ODEs | Model | Total sample | Sub-sample | Epoch | σ^2 | γ |
|--|----------|--------------|------------|-------|------------|-----------------|
| | NLS-SVMs | 300 | 20 | 50 | 1 | 10 ⁶ |
| $\frac{}{Problem7}$ | PINN | 1000 | - | 10000 | - | - |
| Problem (| LS-SVMs | 1000 | - | - | 1 | 10^{7} |
| | NLS-SVMs | 1000 | 50 | - | 1 | 10^{7} |
| $\phantom{aaaaaaaaaaaaaaaaaaaaaaaaaaaaaaaaaaa$ | PINN | 1000 | - | 20000 | - | - |
| r rootem 8 | LS-SVMs | 1000 | - | - | 1 | 10^{7} |
| | NLS-SVMs | 1000 | 50 | - | 1 | 10^{7} |
| Problem~9 | PINN | 1000 | - | 10000 | - | - |
| гтонет в | LS-SVMs | 1000 | 1000 | - | 1 | 10^{7} |
| | NLS-SVMs | 1000 | 50 | - | 1 | 10^{7} |
| $\frac{}{Problem10}$ | PINN | 1000 | - | 10000 | - | - |
| Prootem 10 | LS-SVMs | 1000 | - | - | 1 | 10^{7} |
| | NLS-SVMs | 1000 | 50 | - | 1 | 10^{7} |
| $\overline{Problem 11}$ | PINN | 1000 | - | 10000 | - | - |
| | LS-SVMs | 1000 | - | - | 1 | 10^{7} |
| | NLS-SVMs | 1000 | 20 | - | 1 | 10^{7} |
| $\frac{}{Problem12}$ | PINN | 1000 | - | 10000 | - | - |
| rrootem 12 | LS-SVMs | 1000 | - | - | 1 | 10^{7} |
| | NLS-SVMs | 1000 | 20 | - | 1 | 10^{7} |
| ${Problem13}$ | PINN | 1000 | - | 10000 | - | - |
| 1 rootem 13 | LS-SVMs | 1000 | - | - | 1 | 10^{7} |
| | NLS-SVMs | 1000 | 20 | - | 1 | 10^{7} |
| $\overline{Problem14}$ | PINN | 200 | - | 10000 | - | - |
| 1 rootem 14 | LS-SVMs | 200 | - | 500 | 1 | 10^{7} |
| | NLS-SVMs | 200 | 10 | 500 | 1 | 10^{7} |
| $\frac{}{Problem15}$ | PINN | 300 | - | 20000 | - | - |
| F 700tem 15 | LS-SVMs | 300 | - | 400 | 1 | 10^{7} |
| | NLS-SVMs | 300 | 10 | 400 | 1 | 10^{7} |
| $\phantom{aaaaaaaaaaaaaaaaaaaaaaaaaaaaaaaaaaa$ | PINN | 1000 | - | 10000 | - | - |
| Froniem 16 | LS-SVMs | 1000 | - | - | 1 | 10^{7} |
| | NLS-SVMs | 1000 | 20 | - | 1 | 10^{7} |

Table 10: Hyperparameter configuration for NLS-SVMs in large-scale ODEs solving

| ODEs | Model | t | Total sample | Sub-sample | σ^2 | γ |
|-------------------------|----------|---------|--------------|------------|------------|----------|
| $\overline{Problem1}$ | NLS-SVMs | [0,100] | 50000 | 200 | 10 | 10^{7} |
| $\overline{Problem\ 3}$ | NLS-SVMs | [0,100] | 50000 | 200 | 10 | 10^{7} |
| $\overline{Problem\ 5}$ | NLS-SVMs | [0,100] | 10000 | 100 | 8 | 10^{6} |
| $\overline{Problem\ 7}$ | NLS-SVMs | [0,100] | 50000 | 100 | 1 | 10^{7} |
| $\overline{Problem~8}$ | NLS-SVMs | [0,50] | 20000 | 200 | 1 | 10^{7} |
| $\overline{Problem~9}$ | NLS-SVMs | [0,100] | 50000 | 200 | 1 | 10^{7} |
| $\overline{Problem~10}$ | NLS-SVMs | [0,100] | 50000 | 200 | 1 | 10^{7} |
| $\overline{Problem11}$ | NLS-SVMs | [0,100] | 50000 | 200 | 1 | 10^{7} |
| Problem~12 | NLS-SVMs | [0,100] | 50000 | 200 | 1 | 10^{7} |

B.6 Assessment of NLS-SVMs for long-time integration of ODEs

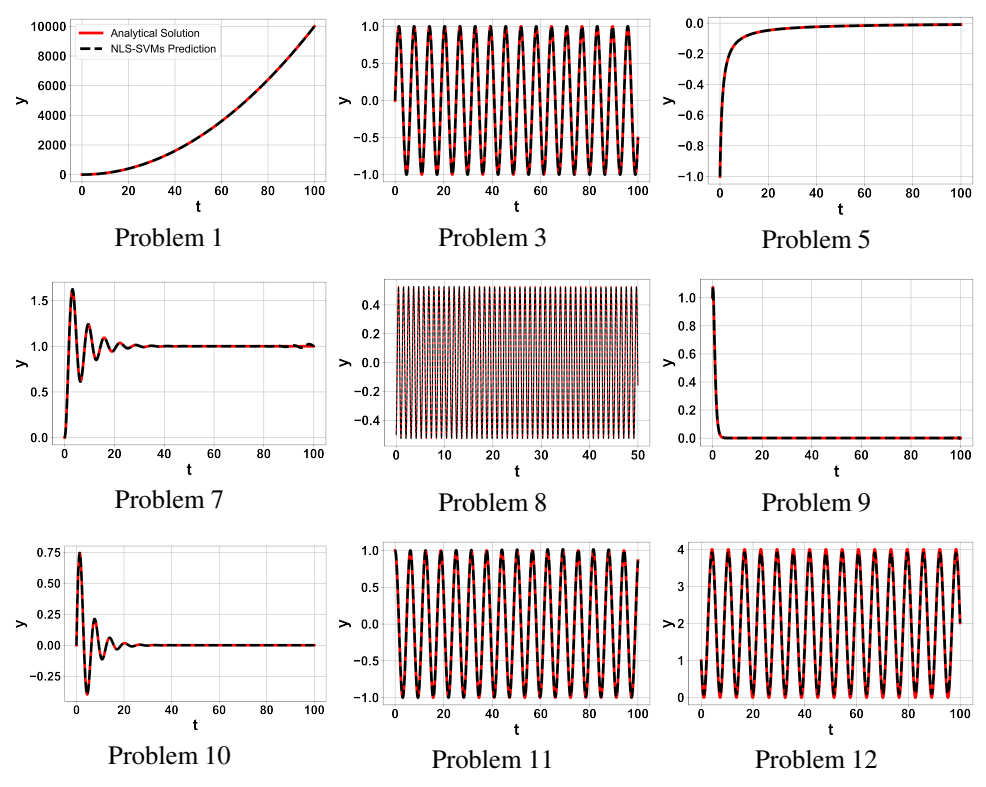


Figure 5: NLS-SVMs predictions against analytical solutions for twelve benchmark problems

B.7 Performance comparison of PINN, LS-SVMs and NLS-SVMs

Table 11: Comparative performance evaluation of PINN, LS-SVMs, and NLS-SVMs in solving ODEs: accuracy metrics and computational efficiency

| ODEs | Model | \mathbb{R}^2 | MAE | RMSE | $\ y - \hat{y}\ _{\infty}$ | Time/s |
|-------------------------|----------|----------------|-----------------------|-----------------------|----------------------------|---------|
| Problem 1 | PINN | 0.99999 | 4.45×10 ⁻³ | 5.05×10 ⁻³ | 9.91×10 ⁻³ | 672.00 |
| | LS-SVMs | 0.99999 | 4.81×10 ⁻⁴ | 5.72×10 ⁻⁴ | 1.17×10 ⁻³ | 9.79 |
| | NLS-SVMs | 0.99999 | 7.94×10 ⁻⁴ | 9.47×10 ⁻⁴ | 1.87×10 ⁻³ | 0.55 |
| Problem 2 | PINN | 0.99989 | 2.03×10 ⁻³ | 2.09×10 ⁻³ | 3.26×10 ⁻³ | 403.00 |
| | LS-SVMs | 0.99999 | 6.87×10 ⁻⁷ | 8.55×10 ⁻⁷ | 3.07×10 ⁻⁶ | 1587.00 |
| | NLS-SVMs | 0.99999 | 3.16×10 ⁻⁶ | 3.77×10 ⁻⁶ | 9.75×10 ⁻⁶ | 0.55 |
| $\overline{Problem~3}$ | PINN | 0.74911 | 1.82×10 ⁻¹ | 2.88×10 ⁻¹ | 1.03×10 ⁰ | 1209.00 |
| | LS-SVMs | 0.99999 | 2.55×10 ⁻⁸ | 3.23×10 ⁻⁸ | 1.36×10 ⁻⁷ | 1879.00 |
| | NLS-SVMs | 0.99999 | 2.06×10 ⁻⁸ | 2.77×10 ⁻⁸ | 1.40×10 ⁻⁷ | 0.56 |
| $\overline{Problem4}$ | PINN | 0.94554 | 5.35×10 ⁻¹ | 7.21×10 ⁻¹ | 1.81×10 ⁰ | 496.00 |
| | LS-SVMs | 0.99999 | 5.26×10 ⁻⁵ | 7.80×10 ⁻⁵ | 2.13×10 ⁻⁴ | 3774.00 |
| | NLS-SVMs | 0.99999 | 5.47×10 ⁻⁴ | 6.92×10 ⁻⁴ | 1.50×10 ⁻³ | 10.20 |
| $\overline{Problem\ 5}$ | PINN | 0.99995 | 1.03×10 ⁻³ | 1.04×10 ⁻³ | 1.13×10 ⁻³ | 166.00 |
| | LS-SVMs | 0.99994 | 8.89×10 ⁻⁴ | 1.11×10 ⁻³ | 1.84×10 ⁻³ | 9.71 |
| | NLS-SVMs | 0.99994 | 8.79×10 ⁻⁴ | 1.07×10 ⁻³ | 1.67×10 ⁻³ | 0.97 |
| Problem 6 | PINN | 0.89021 | 1.47×10 ⁻² | 1.76×10 ⁻² | 3.57×10 ⁻² | 75.60 |
| | LS-SVMs | 0.99993 | 4.47×10 ⁻⁴ | 5.11×10 ⁻⁴ | 8.63×10 ⁻⁴ | 13.20 |
| | NLS-SVMs | 0.99974 | 8.89×10 ⁻⁴ | 1.01×10 ⁻³ | 1.70×10 ⁻³ | 0.69 |

| ODEs | Model | \mathbb{R}^2 | MAE | RMSE | $\ y - \hat{y}\ _{\infty}$ | Time/s |
|--------------------------|----------|----------------|-----------------------|-----------------------|----------------------------|---------|
| Problem 7 | PINN | 0.91449 | 6.58×10 ⁻² | 8.06×10 ⁻² | 1.63×10 ⁻¹ | 1021.00 |
| rrootem i | LS-SVMs | 0.99997 | 1.43×10^{-3} | 1.66×10^{-3} | 3.02×10^{-3} | 22.90 |
| | NLS-SVMs | 0.99997 | 1.43×10^{-3} | 1.67×10^{-3} | 3.02×10^{-3} | 0.50 |
| $\overline{Problem~8}$ | PINN | 0.99973 | 5.23×10 ⁻³ | 5.92×10 ⁻³ | 1.04×10 ⁻² | 1392.00 |
| 1 rootem 8 | LS-SVMs | 0.99999 | 7.14×10^{-6} | 8.93×10 ⁻⁶ | 2.86×10^{-5} | 20.80 |
| | NLS-SVMs | 0.99999 | 5.66×10^{-5} | 7.05×10^{-5} | 2.23×10^{-4} | 0.44 |
| $\overline{Problem 9}$ | PINN | 0.99999 | 8.66×10 ⁻⁵ | 9.96×10 ⁻⁵ | 1.89×10 ⁻⁴ | 776.00 |
| 1 rootent s | LS-SVMs | 0.99999 | 1.60×10^{-5} | 1.92×10^{-5} | 6.20×10^{-5} | 20.20 |
| | NLS-SVMs | 0.99999 | 5.74×10^{-5} | 6.92×10^{-5} | 2.21×10^{-4} | 0.47 |
| $\overline{Problem10}$ | PINN | 0.98291 | 3.12×10 ⁻² | 4.07×10 ⁻² | 8.62×10 ⁻² | 636.00 |
| 1 rootem 10 | LS-SVMs | 0.99999 | 9.40×10 ⁻⁹ | 1.34×10^{-8} | 3.99×10^{-8} | 24.70 |
| | NLS-SVMs | 0.99999 | 4.29×10^{-8} | 6.06×10^{-8} | 3.09×10^{-8} | 0.49 |
| $\overline{Problem\ 11}$ | PINN | 0.99999 | 1.62×10 ⁻⁵ | 1.89×10 ⁻⁵ | 3.32×10 ⁻⁵ | 817.00 |
| | LS-SVMs | 0.99999 | 2.81×10^{-8} | 3.48×10^{-8} | 1.16×10^{-7} | 16.30 |
| | NLS-SVMs | 0.99999 | 2.36×10^{-9} | 2.97×10^{-9} | 9.43×10 ⁻⁹ | 0.45 |
| $\overline{Problem12}$ | PINN | 0.99999 | 2.28×10 ⁻⁵ | 2.29×10 ⁻⁵ | 2.60×10 ⁻⁵ | 969.00 |
| 1 rootem 12 | LS-SVMs | 0.99999 | 1.56×10^{-8} | 1.93×10 ⁻⁸ | 5.91×10^{-8} | 16.70 |
| | NLS-SVMs | 0.99999 | 3.15×10^{-9} | 3.94×10^{-9} | 1.31×10^{-8} | 0.46 |
| $\overline{Problem13}$ | PINN | 0.99987 | 4.22×10 ⁻³ | 5.72×10 ⁻³ | 1.05×10 ⁻² | 1475.00 |
| 1 rootem 13 | LS-SVMs | 0.99999 | 2.77×10^{-7} | 3.42×10^{-7} | 9.56×10^{-7} | 33.60 |
| | NLS-SVMs | 0.99999 | 3.48×10^{-7} | 4.36×10^{-7} | 1.45×10^{-6} | 0.48 |
| $\overline{Problem 14}$ | PINN | 0.99999 | 8.22×10 ⁻⁶ | 8.77×10 ⁻⁶ | 1.34×10 ⁻⁵ | 112.40 |
| 1 rootem 14 | LS-SVMs | 0.99999 | 7.38×10^{-7} | 9.17×10 ⁻⁷ | 2.02×10^{-6} | 36.00 |
| | NLS-SVMs | 0.99999 | 1.17×10^{-6} | 1.57×10^{-6} | 3.85×10^{-6} | 1.39 |
| Problem 15 | PINN | 0.99774 | 2.42×10 ⁻³ | 2.62×10 ⁻³ | 3.62×10 ⁻³ | 230.00 |
| 1 rootem 15 | LS-SVMs | 0.99999 | 2.14×10^{-8} | 2.66×10^{-8} | 6.68×10^{-7} | 85.40 |
| | NLS-SVMs | 0.99999 | 1.68×10^{-7} | 1.98×10^{-7} | 3.46×10^{-7} | 3.25 |
| Problem 16 | PINN | 0.99812 | 1.24×10 ⁻² | 1.35×10 ⁻² | 1.80×10 ⁻² | 2699.00 |
| 1 rootem 10 | LS-SVMs | 0.99999 | 1.50×10^{-4} | 1.88×10^{-4} | 6.84×10^{-4} | 24.30 |
| | NLS-SVMs | 0.99999 | 1.72×10^{-5} | 2.06×10^{-5} | 5.07×10^{-5} | 0.42 |

Table 12: Performance evaluation of NLS-SVMs for long-time integration of ODEs: accuracy and computational efficiency

| ODEs | Model | R^2 | MAE | RMSE | $\ y - \hat{y}\ _{\infty}$ | Time/s |
|-------------------------|----------|---------|-----------------------|-----------------------|----------------------------|--------|
| $\overline{Problem\ 1}$ | NLS-SVMs | 0.99999 | 1.38×10 ⁻⁴ | 4.23×10 ⁻⁴ | 4.40×10 ⁻³ | 34.80 |
| $\overline{Problem~3}$ | NLS-SVMs | 0.99999 | 5.95×10 ⁻⁸ | 1.18×10 ⁻⁷ | 1.76×10 ⁻⁶ | 24.20 |
| $\overline{Problem\ 5}$ | NLS-SVMs | 0.99999 | 9.96×10 ⁻⁵ | 2.36×10 ⁻⁴ | 2.70×10 ⁻³ | 413 |
| $\overline{Problem\ 7}$ | NLS-SVMs | 0.99911 | 1.59×10 ⁻³ | 4.01×10 ⁻³ | 2.36×10 ⁻² | 299.00 |
| $\overline{Problem~8}$ | NLS-SVMs | 0.99999 | 4.09×10 ⁻⁴ | 5.08×10 ⁻⁴ | 1.71×10 ⁻³ | 24.70 |
| $\overline{Problem~9}$ | NLS-SVMs | 0.99996 | 2.55×10 ⁻⁴ | 6.31×10 ⁻⁴ | 6.33×10 ⁻³ | 459.00 |
| $\overline{Problem~10}$ | NLS-SVMs | 0.99999 | 2.72×10 ⁻⁵ | 5.47×10 ⁻⁵ | 3.49×10 ⁻⁴ | 460.00 |
| $\overline{Problem11}$ | NLS-SVMs | 0.99981 | 7.85×10 ⁻³ | 9.62×10 ⁻³ | 1.55×10 ⁻² | 372.00 |
| Problem 12 | NLS-SVMs | 0.99709 | 6.55×10 ⁻² | 7.27×10 ⁻² | 1.05×10 ⁻¹ | 379.00 |

B.8 Performance improvements

 $\begin{tabular}{ll} Table 13: Benchmarking NLS-SVMs against PINN and LS-SVMs on ODE problems: accuracy and speed \end{tabular}$

| Model | ΔR^2 | $\Delta MAE/\%$ | $\Delta RMSE/\%$ | $\Delta \left\ y - \hat{y} \right\ _{\infty} / \%$ | Speedup |
|---|---|--|--|--|------------------|
| NLS-SVMs vs PINN | +0.00000 | $\downarrow 3.66 \times 10^{-1}$ | $\downarrow 4.10 \times 10^{-1}$ | $\downarrow 8.04 \times 10^{-1}$ | ↑ 1222 |
| NLS-SVMs vs LS-SVMs | +0.00000 | $\uparrow 3.13 \times 10^{-2}$ | $\uparrow 3.75 \times 10^{-2}$ | $\uparrow 7.00 \times 10^{-2}$ | ↑ 18 |
| NLS-SVMs vs PINN | +0.00010 | $\downarrow 2.03 \times 10^{-1}$ | $\downarrow 2.09 \times 10^{-1}$ | $\downarrow 3.25 \times 10^{-1}$ | ↑ 733 |
| NLS-SVMs vs LS-SVMs | +0.00000 | $\uparrow 2.47 \times 10^{-4}$ | $\uparrow 2.92 \times 10^{-4}$ | $\uparrow 6.68 \times 10^{-4}$ | ↑ 2885 |
| NLS-SVMs vs PINN NLS-SVMs vs LS-SVMs | +0.25088 +0.00000 | $\downarrow 1.82 \times 10^{1}$ $\downarrow 4.90 \times 10^{-7}$ | $ \downarrow 2.88 \times 10^{1} $ $ \downarrow 4.60 \times 10^{-7} $ | $\downarrow 1.03 \times 10^2$ $\uparrow 4.00 \times 10^{-7}$ | ↑ 2159 ↑ 3355 |
| NLS-SVMs vs PINN NLS-SVMs vs LS-SVMs | +0.05445 +0.00000 | $ \downarrow 5.34 \times 10^{1} $ $ \uparrow 4.94 \times 10^{-2} $ | $ \downarrow 7.20 \times 10^{1} $ $ \uparrow 6.14 \times 10^{-2} $ | $\downarrow 1.81 \times 10^2$ $\uparrow 1.29 \times 10^{-1}$ | ↑ 49 ↑ 370 |
| NLS-SVMs vs PINN | -0.00001 | $\downarrow 1.51 \times 10^{-2}$ | $\uparrow 3.00 \times 10^{-4}$ | $\uparrow 5.40 \times 10^{-2}$ | ↑ 171 |
| NLS-SVMs vs LS-SVMs | +0.00000 | $\downarrow 1.00 \times 10^{-3}$ | $\downarrow 4.00 \times 10^{-3}$ | $\downarrow 1.70 \times 10^{-2}$ | ↑ 10 |
| NLS-SVMs vs PINN | -0.10953 | $\downarrow 1.38 \times 10^{0}$ | $\downarrow 1.66 \times 10^{0}$ | $\begin{array}{c} \downarrow 3.40 \times 10^{0} \\ \uparrow 8.37 \times 10^{-2} \end{array}$ | ↑ 190 |
| NLS-SVMs vs LS-SVMs | -0.00019 | $\uparrow 4.42 \times 10^{-2}$ | $\uparrow 4.99 \times 10^{-2}$ | | ↑ 19 |
| NLS-SVMs vs PINN NLS-SVMs vs LS-SVMs | +0.08548 +0.00000 | $ \downarrow 6.44 \times 10^{0} \uparrow 0.00 \times 10^{0} $ | 1.00×10^{0} 1.00×10^{-3} | $\downarrow 1.60 \times 10^{1}$ $\uparrow 0.00 \times 10^{0}$ | ↑ 2042 ↑ 46 |
| NLS-SVMs vs PINN | +0.00026 | $\downarrow 5.17 \times 10^{-1}$ | $\downarrow 5.85 \times 10^{-1}$ | $\downarrow 1.02 \times 10^{0}$ | ↑ 3164 |
| NLS-SVMs vs LS-SVMs | +0.00000 | $\uparrow 4.95 \times 10^{-2}$ | $\uparrow 6.16 \times 10^{-3}$ | $\uparrow 1.94 \times 10^{-2}$ | ↑ 47 |
| NLS-SVMs vs PINN | +0.00000 | $\downarrow 2.92 \times 10^{-3}$ | $\downarrow 3.04 \times 10^{-3}$ | $\uparrow 3.20 \times 10^{-3}$ | ↑ 1651 |
| NLS-SVMs vs LS-SVMs | | $\uparrow 4.14 \times 10^{-3}$ | $\uparrow 5.00 \times 10^{-3}$ | $\uparrow 1.59 \times 10^{-2}$ | ↑ 43 |
| NLS-SVMs vs PINN | +0.01708 | $\downarrow 3.12 \times 10^{0}$ | 4.07×10^{0} | $\downarrow 8.62 \times 10^{0}$ | ↑ 1298 |
| NLS-SVMs vs LS-SVMs | +0.00000 | $\uparrow 3.35 \times 10^{-6}$ | 4.72×10^{-6} | $\downarrow 9.00 \times 10^{-7}$ | ↑ 50 |
| NLS-SVMs vs PINN | +0.00000 +0.00000 | $\downarrow 1.62 \times 10^{-3}$ | $\downarrow 1.90 \times 10^{-3}$ | $\downarrow 3.32 \times 10^{-3}$ | ↑ 1816 |
| NLS-SVMs vs LS-SVMs | | $\downarrow 2.57 \times 10^{-6}$ | $\downarrow 3.18 \times 10^{-6}$ | $\downarrow 1.07 \times 10^{-5}$ | ↑ 36 |
| NLS-SVMs vs PINN | +0.00000 +0.00000 | $\downarrow 2.28 \times 10^{-3}$ | $\downarrow 2.29 \times 10^{-3}$ | $\downarrow 2.60 \times 10^{-3}$ | ↑ 2107 |
| NLS-SVMs vs LS-SVMs | | $\downarrow 1.25 \times 10^{-6}$ | $\downarrow 1.54 \times 10^{-6}$ | $\downarrow 4.60 \times 10^{-6}$ | ↑ 36 |
| NLS-SVMs vs PINN | +0.00012 | $\downarrow 4.22 \times 10^{-1}$ | $\downarrow 5.72 \times 10^{-1}$ | $\downarrow 1.05 \times 10^{0}$ | ↑ 3073 |
| NLS-SVMs vs LS-SVMs | +0.00000 | $\uparrow 7.10 \times 10^{-6}$ | $\uparrow 9.40 \times 10^{-6}$ | $\uparrow 4.94 \times 10^{-5}$ | ↑ 70 |
| NLS-SVMs vs PINN | +0.00000 | $\downarrow 7.05 \times 10^{-4}$ | $\downarrow 7.20 \times 10^{-4}$ | $\downarrow 9.55 \times 10^{-4}$ | ↑ 81 |
| NLS-SVMs vs LS-SVMs | | $\uparrow 4.32 \times 10^{-5}$ | $\uparrow 6.53 \times 10^{-5}$ | $\uparrow 1.83 \times 10^{-4}$ | ↑ 26 |
| NLS-SVMs vs PINN | +0.00225 | $\downarrow 2.42 \times 10^{-1}$ | $\downarrow 2.62 \times 10^{-1}$ | $\downarrow 3.62 \times 10^{-1} \\ \downarrow 3.22 \times 10^{-5}$ | ↑ 71 |
| NLS-SVMs vs LS-SVMs | +0.00000 | $\uparrow 1.47 \times 10^{-5}$ | $\uparrow 1.71 \times 10^{-5}$ | | ↑ 26 |
| NLS-SVMs vs PINN | +0.00187 | $\downarrow 1.24 \times 10^{0}$ | $\downarrow 1.35 \times 10^{0}$ | $\downarrow 1.79 \times 10^{0}$ | ↑ 6426 |
| NLS-SVMs vs LS-SVMs | +0.00000 | $\downarrow 1.33 \times 10^{-2}$ | $\downarrow 1.64 \times 10^{-2}$ | $\downarrow 6.33 \times 10^{-2}$ | ↑ 58 |
| | NLS-SVMs vs PINN NLS-SVMs vs LS-SVMs NLS-SVMs vs PINN | NLS-SVMs vs PINN +0.00000 NLS-SVMs vs LS-SVMs +0.00000 NLS-SVMs vs PINN +0.00000 NLS-SVMs vs PINN +0.00000 NLS-SVMs vs PINN +0.25088 NLS-SVMs vs PINN +0.05445 NLS-SVMs vs PINN +0.00000 NLS-SVMs vs PINN +0.00000 NLS-SVMs vs PINN -0.00001 NLS-SVMs vs PINN -0.10953 NLS-SVMs vs PINN +0.08548 NLS-SVMs vs LS-SVMs +0.00000 NLS-SVMs vs PINN +0.00026 NLS-SVMs vs LS-SVMs +0.00000 NLS-SVMs vs LS-SVMs +0.00000 NLS-SVMs vs LS-SVMs +0.00000 NLS-SVMs vs PINN +0.00000 NLS-SVMs vs PINN +0.00000 NLS-SVMs vs LS-SVMs +0.00000 NLS-SVMs vs PINN +0.00000 NLS-SVMs vs PINN | NLS-SVMs vs PINN | NLS-SVMs vs PINN | NLS-SVMs vs PINN |